KTH Chemical Science
and Engineering

SELF ASSEMBLY OF SURFACTANTS AND POLYELECTROLYTES IN SOLUTIONS AND AT INTERFACES

Luis Alejandro Bastardo

Doctoral Thesis at the Royal Institute of Technology

Stockholm 2005

Akademisk avhandling som med tillstånd av Kungl. Tekniska Högskolan framlägges till offentlig granskning för avläggande av teknisk doktorexamen fredagen den 30 september 2005 klockan 9.00 i sal D3, KTH, Lindstedsv. 17, Stockholm.

Luis Alejandro Bastardo. *Self Assembly of Surfactants and Polyelectrolytes in Solutions and at Interfaces*

TRITA-YTK-0502
ISSN: 1650-0490
ISBN: 91-7178-127-7

ABSTRACT

This thesis focuses on the study of the interactions between polyelectrolytes and surfactants in aqueous solutions and at interfaces, as well as on the structural changes these molecules undergo due to that interaction. Small–angle neutron scattering, dynamic, and static light scattering were the main techniques used to investigate the interactions in bulk.

The first type of polymer studied was a negatively charge glycoprotein (mucin); its interactions with ionic sodium alkyl sulfate surfactants and nonionic surfactants were determined. This system is of great relevance for several applications such as oral care and pharmaceutical products, since mucin is the main component of the mucus layer that protects the epithelial surfaces (e.g. oral tissues). Sodium dodecyl sulfate (SDS) on the other hand, has been used as foaming agent in tooth pastes for a very long time. In this work it is seen how SDS is very effective in dissolving the large aggregates mucin forms in solution, as well as in removing preadsorbed mucin layers from different surfaces. On the other hand, the nonionic surfactant *n*-dodecyl β-D-maltopyranoside (C_{12}-mal), does not affect significantly the mucin aggregates in solution, neither does it remove mucin effectively from a negatively charge hydrophilic surface (silica). It can be suggested that nonionic surfactants (like the sugar–based C_{12}-mal) could be used to obtain milder oral care products.

The second type of systems consisted of positively charged polyelectrolytes and a negatively charged surfactant (SDS). These systems are relevant to a wide variety of applications ranging from mining and cleaning to gene delivery therapy. It was found that the interactions of these polyelectrolytes with SDS depend strongly on the polyelectrolyte structure, charge density and the solvent composition (pH, ionic strength, and so on). Large solvent isotopic effects were found in the interaction of polyethylene imine (PEI) and SDS, as well as on the interactions of this anionic surfactant and the sugar–based *n*-decyl β-D-glucopyranoside ($C_{10}G_1$). These surfactants mixtures formed similar structures in solutions to the ones formed by some of the polyelectrolytes studied, i.e. ellipsoidal micelles at low electrolyte concentration and stiff rods, at high electrolyte and SDS concentrations.

Key words

Surfactant, polyelectrolyte, small–angle neutron scattering, static light scattering, dynamic light scattering, polyelectrolyte–surfactant association, protein, protein – surfactant association, surface tension, electrophoretic mobility, isotopic effects.

SAMMANFATTNING

Den här avhandlingen behandlar främst studierna av växelverkan mellan polyelektrolyter och tensider i vattenlösning och på ytor, samt vilka strukturella förändringar dessa molekyler genomgår till följd av denna växelverkan. För att studera växelverkan i lösning användes huvudsakligen teknikerna lågvinkel neutronspridning samt dynamisk och statisk ljusspridning.

Det första systemet som studerades var ett negativt laddat protein (mucin) och dess växelverkan med joniska natrium alkylsulfat tensider och nonjoniska tensider. Systemet är av stor betydelse för ett flertal applikationer, såsom orala hygien- och farmaceutiska produkter, eftersom mucin är huvudkomponenten i mucusskiktet som skyddar slemhinnans ytor (t ex orala vävnader). Natrium dodecylsulfat (SDS) har däremot använts som skummedel i tandkräm under lång tid. I detta arbete har det visats sig att SDS väldigt effektivt löser upp stora aggregat av mucin i lösning, samt desorberar mucinskikt från olika ytor. Emellertid påverkas inte mucinaggregaten i lösning nämnvärt av den nonjoniska tensiden *n*-dodecyl-β-D-maltopyranosid (C_{12}-mal). Den tensider tar inte heller bort mucin från negativt laddade hydrofila ytor (kisel). Slutsatsen blir att användningen av nonjoniska tensider (såsom den sockerbaserade C_{12}-mal) leder till utveckling av mildare orala hygienprodukter.

Det andra systemet inkluderar positivt laddade polyelektrolyter och negativt laddade tensider (SDS). Systemen är relevanta för en omfattande mängd av applikationer, vilka sträcker sig från gruvdrift och rengörning till genterapi. I arbetet upptäcktes det att växelverkan mellan dessa polyelektrolyter och SDS är starkt beroende av struktur, laddningsdensitet samt på lösningsmedlets sammansättning (pH, jonstyrka och så vidare). En storisotop effekt i lösningsmedel observerades för växelverkan mellan polyetylenimin (PEI) och SDS, i likhet med växelverkan mellan denna anjoniska tensid och den sockerbaserade tensiden *n*-decyl-β-D-maltopyranosid ($C_{12}G_1$). Dessa tensider bildar liknande strukturer i lösning som de som bildades av några av de polyelektrolyter som studerades, t ex elliptiska miceller i låg halt av elektrolyt och stela cylindrar i hög koncentration av salt och SDS.

RESUMEN

En este trabajo se estudia las interacciones entre polielectrolitos y surfactantes en medio acuoso y en interfaces aire-líquido y líquido-sólido. Se hace énfasis en los cambios estructurales que ocurren en estas moléculas debido a interacciones en solución medidas por técnicas de difracción de neutrones a pequeño ángulo, y difracción de luz.

El primer polímero estudiado fue mucina, una proteína con carga negativa, así como sus interacciones con surfactantes alquil sulfonados y noiónicos. Este sistema es de gran relevancia en formulaciones y aplicaciones que incluyen el cuidado oral y el uso de productos farmacéuticos. La mucina es el principal componente de la capa de moco que protege las superficies epiteliales, como los tejidos en la cavidad oral. El dodecil sulfato de sodio (SDS), por su parte, ha sido utilizado por mucho tiempo como agente espumante en dentríficos. En este estudio se pudo observar la efectividad del dodecil sulfato de sodio en la disolución de agregados grandes de mucina en solución, así como en la remoción de las capas de mucina preadsorbida en diferentes superficies. Por otra parte, se encontró que el surfactante no iónico *n*-dodecil β-D-matopiranosa (C_{12}-mal), no afecta de manera significante a los agregados de mucina y no es capaz de remover la mucina de superficies hidrofílicas con carga negativa (como la sílica). Se sugiere entonces que los surfactantes noiónicos (como el C_{12}-mal) pueden ser usados para obtener productos para el cuidado oral mas suaves, menos tóxicos e irritantes.

El segundo tipo de sistemas estudiado consistió en polielectrolitos con carga positiva y SDS. Estos sistemas son relevantes en una gran variedad de aplicaciones que van desde la minería, detergencia y limpieza, hasta la terapia génica. Se observó que las interacciones entre estos polielectrolitos y el SDS dependen fuertemente en la estructura del polielectrolito, su densidad de carga y la composición del solvente (pH, fuerza iónica, etc.). Se observaron importantes efectos isotópicos en la interacción de la polietilen imina (PEI) y SDS, así como en las interacciones entre este surfactante aniónico y el surfactante glucosídico *n*-decil β-D-glucopiranosa ($C_{10}G_1$). Estas mezclas de surfactantes forman en solución estructuras similares a las formadas por algunos de los polielectrolitos estudiados, incluyendo micelas elipsoidales a bajas concentraciones de electrolito y estructuras cilíndricas rígidas, a altas concentraciones de sal y SDS.

CONTENTS

1 LIST OF PAPERS

This thesis is based on the following seven papers, which will be referred to by their roman numerals:

Paper I. Bastardo, L.; Claesson, P. and Brown, W. *Interactions between Mucin and Alkyl Sodium Sulfates in Solution. A Light Scattering Study.* Langmuir, 2002. **18**(10): p. 3848-3853.

Paper II. Dedinaite, A. and Bastardo, L. *Interactions between Mucin and Surfactants at Solid-Liquid Interfaces.* Langmuir, 2002. **18**(24): p. 9383-9392.

Paper III. Bastardo, L.A.; Garamus, V.M.; Bergström, M. and Claesson P.M. *The Structures of Complexes between Polyethylene Imine and Sodium Dodecyl Sulfate in D_2O: A Scattering Study.* Journal of Physical Chemistry B, 2005. **109**(1): p. 167-174.

Paper IV. Bastardo, L.A.; Mézáros, R.; Varga, I.; Gilány, T. and Claesson P.M. *Deuterium isotope effects on the interaction between hyperbranched polyethylene imine and an anionic surfactant.* Journal of Physical Chemistry B, 2005. **109**(33): p. 16196-16202.

Paper V. Bergström, L.M.; Bastardo, L.A. and Garamus, V.M. *A Small-Angle Neutron Scattering Study of Micelles Formed in Aqueous Mixtures of Nonionic Alkylglucoside and an Anionic Surfactant.* Journal of Physical Chemistry B, 2005. **109**(25): p. 12387-12393.

Paper VI. Bastardo, L.A.; Iruthayaraj, J.; Lundin, M.; Dedinaite, A.; Vareikis, A.; Makuška, R.; van der Wal, A.; Furó, I.; Garamus; V.M. and Claesson, P.M. *Soluble complexes in aqueous mixtures of low charge density comb polyelectrolytes and oppositely charged surfactants probed by scattering and NMR.* Submitted.

Paper VII. Bastardo, L.A.; Dedinaite, A.; Lundin, M.; Garamus; V.M. and Claesson, P.M. *Chitosan-SDS association probed by Small-Angle Neutron Scattering*. Manuscript.

The author's contribution to the papers is as follows:

I. Major part of planning, experimental work and part of evaluation.

II. Part of planning, experimental work and evaluation. Reflectometry and AFM measurements and data analysis where done by my coauthor.

III. Major part of planning, experimental work and evaluation.

IV. Major part of planning, experimental work and part of evaluation. Mézáros, R.; Varga, I.; and Gilány, T. evaluated the potentiometric data.

V. Part of planning, experimental work and evaluation.

VI. Part of planning, SANS calculations and data analysis. NMR measurements and data analysis were performed by Istvan Furó.

VII. SANS calculations and data analysis

In paper I, III, IV, VI, and VII, the thesis author has written the major part of the manuscripts.

2 SUMMARY OF PAPERS

In **Paper I** the properties of negatively charged mucin in aqueous solution and its interactions with anionic sodium alkyl sulfate surfactants with different chain lengths; sodium octyl sulfate, sodium decyl sulfate and sodium dodecyl sulfate, were investigated. Dynamic light scattering was the main technique used in this study. Mucin was found to form large aggregates in solution with a hydrodynamic radius above 500 nm. These aggregates dissolve when sodium dodecyl sulfate or sodium decyl sulfate is present at concentrations above 0.2 cmc (cmc = critical micellar concentration). However, sodium octyl sulfate is not as effective in dissolving the mucin aggregates. The dependence of the dissolution of the mucin aggregates on the surfactant chain length suggests that the interactions between these molecules are hydrophobically driven. The kinetics of the dissolution process depends on the surfactant concentration; at higher surfactant concentration the dissolution is faster. Finally, it was observed that at high ionic strength, smaller amounts of surfactant were needed to dissolve the mucin aggregates. This can be explained by the screening of the repulsive electrostatic forces by the salt.

The interactions of mucin with sodium dodecyl sulfate (SDS) and with nonionic surfactants, in bulk solution and at solid liquid and air liquid interfaces, were studied in **Paper II**. The nonionic surfactants used were penta(oxyethylene) dodecyl ether ($C_{12}E_5$) and *n*-dodecyl β-D-maltopyranoside (C_{12}-mal). The addition of $C_{12}E_5$ and C_{12}-mal to mucin solutions does not result in a significant variation on the mucin aggregate size in solution. Surface tension isotherms indicate that very limited association of the nonionic surfactants with mucin occurs; while highly surface active complexes of mucin and SDS are present at the interface up to the cmc of the surfactant. All three surfactants were found to be effective in removing pre–adsorbed mucin from hydrophobic surfaces. However, on a negatively charged hydrophilic surface (silica), SDS and $C_{12}E_5$ are very effective in removing pre-adsorbed mucin, while C_{12}-mal is not. In the case of $C_{12}E_5$ competitive adsorption is suggested to be the removal mechanism, whereas in the case of SDS it is due to the formation of SDS/mucin aggregates that are highly soluble in aqueous solution and have a reduced affinity for the surface, compared to pure mucin.

Paper III deals with the association between the hyperbranched polyethylene imine (PEI) and the oppositely charge SDS in solution at two different pH values. Small–angle neutron scattering and static light scattering were used in order to describe the structure of the complexes formed by these molecules in solution. At low pH values and low surfactant concentrations the highly charged PEI forms disk–like aggregates in solution. An increase in the surfactant concentration, results in the formation a more complex three dimensional structure by the aggregates. The presence of these structures gives rise to a Bragg–like peak in the scattering curve, which is an indication of a very well ordered surfactant–polyelectrolyte structure in solution. X–ray diffraction measurements on the precipitate confirmed the existence of an ordered structure corresponding to a lamellar internal organization. At pH 10.1, the PEI has low charge density. SANS measurements under conditions where the surfactant is contrast matched, revealed very small changes in the scattering curves. This suggests that the polyelectrolyte acts as a template onto which surfactant molecules adsorbed. Analysis of SANS and static light scattering curves, from the samples where both PEI and SDS contribute to the scattering, revealed that the structure of the aggregates is consistent with stacked bilayers, but the ordering effect is much less than in the lamellar phase formed at lower pH.

It is clear then, that PEI is very sensitive to the solvent composition (pH). The effects of the isotopic substitution of water with heavy water (D_2O) on PEI and in its association with SDS are investigated in **Paper IV.** Here, potentiometric titrations reveal that in the basic pH range, a considerable higher amount of amine groups are protonated when PEI is dissolved in D_2O compared to H_2O, at the same pH/pD. This difference in charge diminishes gradually with decreasing solution pH, and completely disappears at around pH 4. Electrophoretic mobility measurements show that the mobilities of the PEI/SDS samples dissolved in heavy water at low surfactant concentration are almost twice that of the samples dissolve in water. Moreover, the charge neutralization point of the polyelectrolyte is shifted to higher surfactant concentrations in heavy water. This is consistent with the observation that PEI has a significantly higher charge density in D_2O than in H_2O at this pH range. At the natural pH/pD of the PEI, as well as at pH = 4, both the mobilities of the PEI/SDS complexes and the charge neutralization point are the same in both solvents.

Very large solvent isoptope effects were also observed while studying the formation of micelles by SDS and *n*-decyl β-D-glucopyranoside ($C_{10}G_1$) with static light

scattering and SANS, in **Paper V**. At high ionic strength (100 mM NaCl) and in excess of $C_{10}G_1$, [SDS]/[$C_{10}G_1$] = 1:3, static light scattering measurements showed that the micelles formed in D_2O are five times larger than the micelles formed in H_2O. This was attributed to a higher hydrophobicity of the $C_{10}G_1$ in D_2O compared to in H_2O. SANS and static light scattering data, at these conditions, were best fitted with a model for long flexible worm–like micelles. The data at the same ionic strength but at [SDS]/[$C_{10}G_1$] = 3:1 and 1:1 corresponded to rigid rod structures. At low ionic strength (0 and 10 mM NaCl) the SANS data were best fitted with a model corresponding to prolate ellipsoids of revolution. The long axis of these ellipsoids becomes smaller with increasing mole fraction of SDS in the solution.

In **Paper VI**, the interactions between the low charge comb polyelectrolyte poly(ethylene oxide) monomethylether methacrylate methacryloxyethyl trimethylammonium chloride (PEO_{45}MEMA:METAC-2) and SDS are investigated. Static light scattering, SANS, surface tension measurements, and nuclear magnetic resonance (NMR) were used in order to characterize this system. This polyelectrolyte adopts a stiff rod conformation in solution. The cross section of the rod decreases with increasing temperature, mainly due to the decrease in solvency of the PEO side chains. SDS associates with PEO_{45}MEMA:METAC-2 and forms soluble complexes at all stoichiometries. Cooperative association is found at free surfactant concentrations above 7 mM. The SDS associated to the PEO_{45}MEMA:METAC-2 molecules is found to be distributed in two populations, one is suggested to be moleculary distributed around the comb polymer backbone, and the other as small micellar–like structures at the periphery of the aggregate.

Another cationic polyelectrolyte with a different structure (chitosan), and its association with sodium dodecyl sulfate was investigated using SANS in **Paper VII**. Pure chitosan in solution was found to adopt a Gaussian chain conformation with a persistence length of 63 Å that decreases marginally to 62 Å with the addition of 30 mM NaCl. The addition of SDS results in relatively complex scattering curves which exhibit two distinct slopes and a Bragg–like peak. This peak points to the formation of common SDS/chitosan structures in solution. While the slopes, correspond to different internal organizations at different length–scales. At large length–scales the organization corresponds to mass fractals, whereas at low length–scales corresponds to surface fractals.

3 INTRODUCTION

Polyelectrolyte–surfactant mixtures are used in a wide range of products in several industries from mining, pulp and paper, and cleaning to food and pharmaceutical, just to mention a few. These two kinds of molecules are generally mixed in order to take advantage of the beneficial properties that they can provide. However, sometimes these mixtures can result in undesirable properties. Therefore, getting a fundamental understanding on surfactant and polyelectrolyte systems is necessary in order to help to enhance the beneficial properties they may bring to certain applications, while preventing the undesirable ones. This is why a lot of effort has been dedicated in order to understand these systems, both in solution and at interfaces. However, there is a lack of information on the structure these molecules and/or their aggregates form in solution and how this structural information can help to explain their properties and behavior.

In this work, polyelectrolytes from different origins (biological and chemical), architectures, charge densities and sizes were investigated. The effect of the solvent conditions, such as pH and ionic strength, on their solution conformation and on the interaction between polymer chains and between these polymers and surfactants were evaluated. Scattering techniques, such as static and dynamic light scattering, and small-angle neutron scattering, were selected as main tools because they allow studying the interactions between colloidal particles in solution by directly measuring the changes that these interactions have on the size and shape of the particles.

The use of surface tension and reflectometry allowed the interactions of polyelectrolytes and surfactants at interfaces to be characterized.

3.1 Surfactants

Surfactant is the term used to describe molecules formed by two distinctive parts one that is soluble in water (hydrophilic) and one that is not (hydrophobic). The hydrophilic part of the surfactant is usually called the head and the hydrophobic part the tail.

Surfactants can be classified depending on the charge of their head group. The ones that have a charged head group are called ionic surfactants, while those with an uncharged head group are called nonionic surfactants.[1]

Ionic surfactants can be classified depending on the charge of their head groups as anionic (negatively charged), cationic (positively charged), or zwitterionic (two charged groups of different sign).[1,2]

3.1.a Surfactants in solution

Due to their amphiphilic nature (i.e. hydrophilic/hydrophobic), surfactants are prone to adsorb at surfaces and interfaces formed by two immiscible phases. This adsorption of surfactants at the water air interfaces, for example, helps them to lower their free energy, because it helps them to satisfy their hydrophilic/hydrophobic affinities.[1,2]

The presence of amphiphilic molecules at the interface, results in a reduction of the free energy of the interface, i.e. the surface (interfacial) tension of the system (γ), decreases. This is quantified by the Gibbs adsorption equation:[3]

$$d\gamma = -\Gamma RTd\ ln\, c \qquad (1)$$

where Γ is the surface excess of the component present at the interface ($\Gamma = m / A$), with m moles of surfactants per unit area, A). R is the molar gas constant; T is the temperature and c the surfactant concentration.

Surfactants also form aggregates in solution. In aqueous solutions the formation of aggregates help the hydrophobic part of the surfactant to avoid being in contact with water, lowering the free energy of the molecules. The surfactant aggregation process in solution occurs at the critical micellar concentration (cmc), which is the point from where all surfactants added to the solution start to form part of aggregates, and the concentration of "surfactant monomers" (single surfactant molecules) in solution remains approximately constant.

In the process of aggregation the hydrophobic interactions between the surfactant tails are balanced with the electrostatic repulsions between the head groups (in the case of ionic surfactants). In the case of nonionic surfactants the hydration shell that forms around their head groups, limits the space available for the surfactants to pack.

Both the adsorption and micellization process are affected by several variables like the temperature, pH, the ionic strength, and the charge or size of the head group and the chain length of the surfactant.

3.2 Polyelectrolytes and Proteins

Polyelectrolytes are polymers built up from monomers containing polar and non–polar groups. This polymers dissociate into macroions and counterions in aqueous solution.[4] One of their main characteristics is the low activity coefficient of the counterions, and the stretching of the polymer chain in solution due to the electrostatic repulsion between their charged segments. [5,6]

Proteins, on the other hand, are copolymers built up from amino acids containing polar and non–polar groups, in biological processes inside organisms. The main differences between proteins and polyelectrolytes are that the first are in general less polydisperse (especially globular proteins) than the second ones, and the presence of some surfactants may induce their denaturation.

In the same way as surfactants, most polyelectrolytes are amphiphiles, and as surfactants they tend to form organized structures in solution. However, the structures formed in polyelectrolyte solutions are often very different to those formed by surfactants. The amphiphilic behavior can also be induced by modifying the polyelectrolyte structure, introducing hydrophobic groups or by mixing them with surfactants.

Hydrophobically modified polyelectrolytes can be classified into block copolymers, associating polyelectrolytes (hydrophobic groups have been incorporated in up to 10 mol% of the polyelectrolyte), and polysoaps (higher amount of larger hydrophobic groups have been incorporated to the polyelectrolyte than in the case of associating polyelectrolytes).[4]

3.3 Mixtures of surfactants and polyelectrolytes

Surfactant and polyelectrolyte mixtures have been studied extensively because of the interesting properties they exhibit both from the fundamental chemical/physical/biological and the industrial point of view.[1,4,7-10] Surfactant/polyelectrolyte interactions depend strongly on the polyelectrolyte properties, such as its chemical composition, charge density, location of charges, and backbone flexibility.[4] From all these properties, the most important ones are the chemical composition (hydrophobicity) of the polyelectrolyte and the sign of its electrical charge, being the hydrophobicity of the polyelectrolyte the one that generally determines quantitatively and qualitatively its interaction with surfactants.[11]

Several models have been proposed to describe the interactions between surfactant and polyelectrolyte in solutions, some of them can be found in reviews[7,12] and some will be discussed in this work.

4 SCATTERING METHODS

Scattering techniques such as static and dynamic light scattering and small-angle neutron scattering have been extensively used to investigate the properties of colloidal systems in solution.[13-28] When light (electromagnetic radiation) is directed towards a solution the photons are either absorbed, transmitted (they do not interact with the solution), re-emitted as light of lower frequency (fluorescence, phosphorescence) or scattered. Light scattering from solutions is originated by the spatial and temporal fluctuations of the refractive index in the scattering medium. The intensity of scattered light depends on the wavelength of the incident light, the size and shape of the particles as well as their optical properties, and the angle of observation.

The same principles can be applied to different scattering measurements (neutrons and X-rays) even thought the scattering mechanisms are different. While in neutron scattering the inhomogeneities in the density of nuclei are measured (see below), X-ray scattering measures the inhomogeneities in electron density.[29]

4.1 Static Light Scattering

Incident light on a sample causes the electrons surrounding the nucleus of the different atoms to oscillate about their equilibrium position, creating an oscillating dipole. This dipole works as an antenna that re-emits radiation of the same frequency as that of the stimulating radiation. This scattering is called *elastic scattering* because there is no loss of energy in the process. In the following the scattering object will be called "particle", this term will be used generically to include colloids, micelles, and polyelectrolytes.

4.1.a Rayleigh scattering.

In a static light scattering experiment the intensity of the scattered light (i_s) is measured at different angles θ, with respect to the incident beam, see Figure 4-1.

If the scattering centers are small (i.e. single molecules, gases) compared with the wavelength of the radiation (dimensions $< \lambda/20$), the relation between the incident light and the scattering observed in the *xy* plane is:

$$R_\theta = \frac{i_s r^2}{I_0\left(1+cos^2\,\theta\right)} \tag{2}$$

where r is the distance from the point of scatter to the detector, I_o is the intensity of the incident beam and i_s is the intensity of the scattered light. This equation is known as the Rayleigh ratio (R_θ). It does not apply in the presence of large particles, in the presence of dust or when the molecules absorb the light.

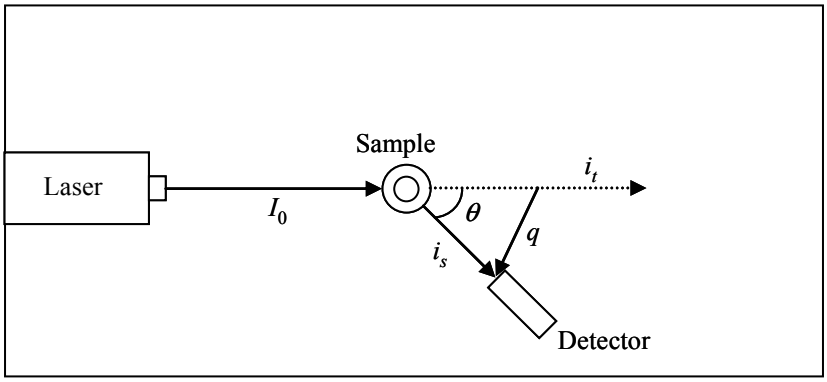

Figure 4-1. *Schematic representation of a light scattering instrument.*

In solutions, the scattering can be due to fluctuations in solvent density (which can be subtracted from the total scattering by using a "blank" sample) and fluctuations in solute concentration. For dilute systems (i.e. where intermolecular interactions are negligible), the Rayleigh ratio can be correlated to the molecular mass (M) and the concentration (c) by the relation:[30]

$$R_\theta = KcM \tag{3}$$

Where K is the optical constant for vertically polarized incident light and is given by:

$$K = \frac{4\pi^2 n^2 \left(dn/dc\right)^2}{N_A \lambda^4} \tag{4}$$

where n is the refractive index of the solvent, dn/dc the refractive index increment of the solute, N_A the Avogadro's number and λ the wavelength of the light.

In real systems, on the other hand, it is necessary to take into account the effect of solute concentration. This can be achieved by relating the scattering behavior to the derivative of the osmotic pressure with concentration (c):[31]

$$\frac{Kc}{R_\theta} = \frac{1}{M} + 2Bc + \ldots \tag{5}$$

where B is the second virial coefficient. This coefficient gives information about the pair interactions between two (colloidal) particles. Negative values of the coefficient denote attractive potentials, while positive values refer to repulsive potentials.[3] In the case of polydisperse systems the weight average molecular weight is the one that is measured by SLS.

4.1.b Debye scattering theory.

The Debye theory is used when the scatterers have dimensions comparable with λ, which is the case in the present work (i.e. polyelectrolytes, colloidal aggregates). This has as a consequence that different parts of the same particle can behave as scattering centers. Because the distances between these centers have the same magnitude as the wave length of light, there will be interference by the waves scattered by different parts of the same molecule.

An interparticle scattering function needs to be included in the light scattering function and the expression for the relation between incident and scattered intensity is modified to:[31]

$$R_\theta = \frac{i_s r^2 P(\theta)}{I_0 (1 + cos^2\,\theta)} \tag{6}$$

where $P(\theta)$ is the form factor, that takes into account interferences between 2 scattering points in a molecule.

$$P(\theta) i_s = i_c \tag{7}$$

with i_c the corrected scattering. For the Debye theory then:

$$\frac{Kc}{R_\theta} = \frac{1}{P(\theta)} \left(\frac{1}{M} + 2Bc \right) \tag{8}$$

At high angles the form factor depends on the nature and shape of the scattering particle (Gaussian coil, rod, sphere, and so on). For a Gaussian coil, for example, the expression of $P(\theta)$ is:

$$P(\theta) = 1 - \frac{1}{3} \left(\frac{4\pi n}{\lambda} \right)^2 R_g \, sin^2 \left(\frac{\theta}{2} \right) \tag{9}$$

Interference effects disappear at $\theta = 0$, but since the intensity of the light can not be measured at $\theta = 0$ because of the transmitted light, measurements at several angles should be performed and then extrapolated to $\theta = 0$ (see below).

4.1.c Zimm plot

If the form factor is written as a function of the scattering vector q:

$$q = \frac{4\pi n}{\lambda} sin\left(\frac{\theta}{2}\right) \tag{10}$$

The following expression is obtained:

$$\frac{1}{P(\theta)} = 1 + \frac{1}{3} R_g^2 q^2 \tag{11}$$

This expression of the form factor is independent of the form of the particles, and can be applied as long as $R_g^2 q^2 < 1$, i.e. at small q, or equivalently, small θ. Here R_g is the radius of gyration of the particle.

By using this expression within the Debye theory, the Zimm plot expression is obtained:

$$\frac{Kc}{R_\theta} = \left(\frac{1}{M} + 2Bc\right)\left(1 + \frac{1}{3} R_g^2 q^2\right) \tag{12}$$

To make use of the Zimm plot expression the sample should be measured at different concentrations and different angles. Then, by plotting data as a function of the square of the scattering vector (i.e. Kc/R_θ vs. q^2), a Zimm plot is obtained.

Each fit of the constant angle data is extrapolated to zero concentration, and each fit at constant concentration is extrapolated to zero angle, obtaining two lines. The average molecular weight (M) is calculated from the intercept of each extrapolated line with the y-axis. R_g is calculated from the slope of the extrapolated line at zero concentration, and the second virial coefficient (B) is calculated from the slope of the extrapolated line at zero angle.[31,32] A Zimm plot can be observed in Figure 4-2.

The radius of gyration calculated with the Zimm plot approximation is a measurement of the particle extension in space, without assuming any specific shape, in other words, R_g is the root mean square distance of the polymer segments from the centre of mass.[33]

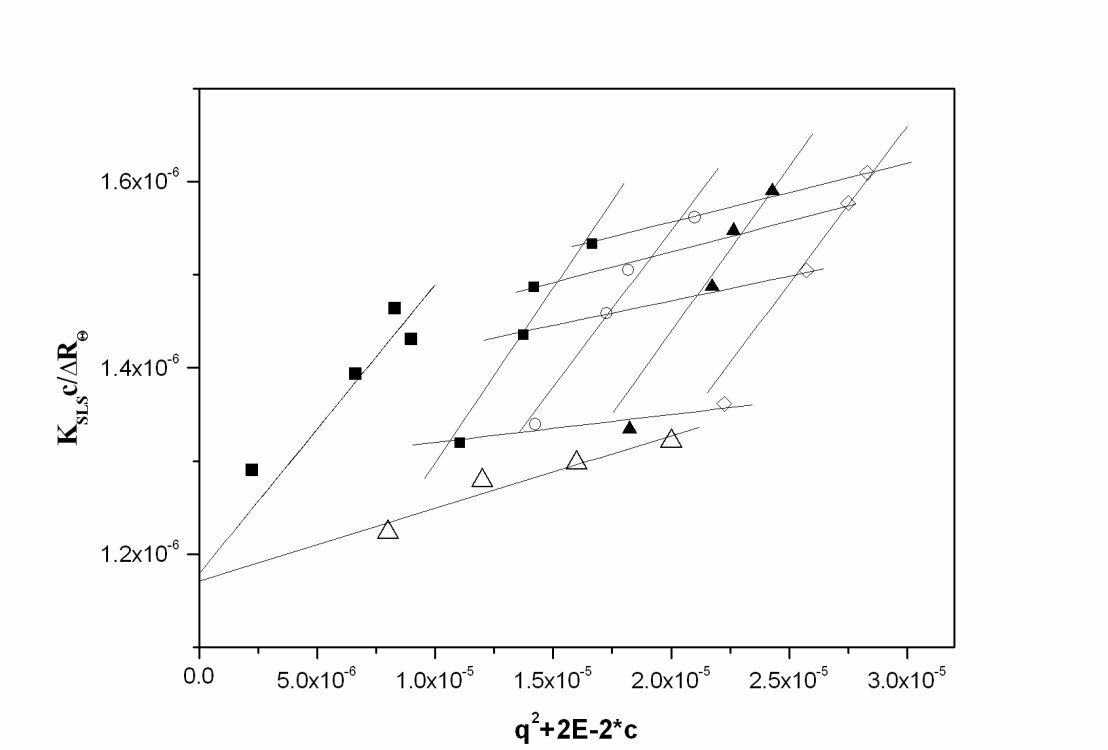

Figure 4-2. *Experimental Zimm plot of PEO_{45}MEMA:METAC-2.*

4.2 Dynamic Light Scattering

In dynamic light scattering (DLS) measurements, the variation of the scattering intensity with time is studied, making possible to get information about the random (Brownian) motion of particles in solution. This diffusion of the molecules from or to the detector, together with their oscillating electrons, generates a *Doppler effect* according to which the observed frequency of a moving transmitting source shifts to higher or lower frequencies depending on its velocity and the direction relative to the detector.[14] As a consequence the scattered intensity fluctuates around an average value.

The intensities are measured at short time intervals Δt (micro– to milliseconds) for long periods of time t (milliseconds to seconds). These experiments are repeated many times (about 10^5 times), to increase the signal to noise ratio. The average of the measurements done at two different time intervals are multiplied and stored. These intensity products define the autocorrelation function:[14]

$$G_2(t) = [I(t).I(t+\Delta t)] \tag{13}$$

where the subscript "2" denotes the *intensity function*, and the brackets denote the product average. At short time differences (Δt), the molecules directions and velocities resemble the ones of the previous time interval. At these conditions the product average has its highest value, close to $<I^2>$. At long times, the molecules will have suffered many collisions and lost all memory of their original velocity and direction. At this point the values of I are completely unrelated and the product will approach $<I>^2$, see Figure 4-3.

$G_2(t)$ is the time correlation function of the scattered intensity, and the characteristic decay time for the process (relaxation time) is τ. However, in practice the intensity normalized time correlation function is used:

$$g_2 = [I(t) \cdot I(t+\Delta t)] / I(t)^2 \tag{14}$$

This function has a value of 1 at small Δt and a value of zero at large Δt.

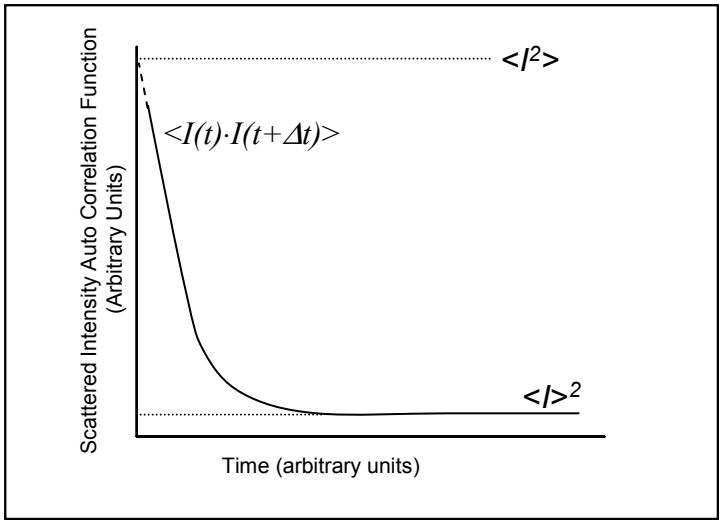

Figure 4-3. *Time average autocorrelation function of the scattered intensity as a function of time.*

The measured intensity time correlation function is related to the normalized correlation function of the *scattered electric field, $g^1(t)$,* by the Siegert relationship:[34]

$$g_2(t) = \left[1 + \beta\left(g^1(t)\right)^2\right] \tag{15}$$

In which β is a constant characteristic of the instrument and is approximately close to one. For monodisperse particles, $g^1(t)$ is a single exponential function:[34]

$$g^1(t) = exp(-\Gamma t) = exp(-Dq^2 t) \tag{16}$$

where Γ is the relaxation rate and D the translational diffusion coefficient.

For small, non-interacting, dilute spheres the Stokes–Einstein relationship can be used to calculate the hydrodynamic radius of the sample:[3,31]

$$D = \frac{k_B T}{6\pi\eta R_H} \tag{17}$$

where k_B is the Boltzmann constant, η is the solvent viscosity and R_H the hydrodynamic radius of the particle.

For polydisperse systems there is a distribution of both Γ and D. The correlation curve obtained in such a case the result of the superposition of many individual contributions. The contribution of each species in DLS is determined by its scattered intensity, resulting in the average diffusion coefficient:

$$\overline{D}_{DLS} = \frac{\Sigma_i I_i D_i}{\Sigma_i I_i} \tag{18}$$

For high molecular weight polymers the scattering intensity is proportional to $c_i M_i P(\theta)_i$, giving an average:

$$\overline{D}_{DLS} = \frac{\Sigma_i c_i M_i P(\theta)_i D_i}{\Sigma_i c_i M_i P(\theta)_i} \tag{19}$$

For small molecules (diameter < 20 nm), $P(\theta) \rightarrow 1$, then:

$$\overline{D}_{DLS} = \frac{\Sigma_i c_i M_i D_i}{\Sigma_i c_i M_i} = \frac{\Sigma_i z_i D_i}{\Sigma_i z_i} = \overline{D}_z \tag{20}$$

that is the *z*-average diffusion coefficient. For larger molecules it is convenient to do the measurements at low angles, in order to minimize the effect of intramolecular interactions ($P(\theta)\rightarrow 1$).

For non-uniform, polydisperse polymers it is preferred to use $g^1(t)$ instead of $g^2(t)$, in data analysis. Then a scattering curve is calculated on the bases of an assumed distribution of decay rates, and this curve is compared with the experimental data. The use of the program CONTIN is widely accepted in order to do these calculations. The solutions given by this program are subjected to two constraints: *a)* it rejects all unreasonable solutions (i.e. the ones with negative values in the distribution), *b)* the principle of parsimony, in which the simplest, smoothest and least detailed solution is less likely to be wrong.[27,31,35]

4.3 Small-Angle Neutron Scattering (SANS)

SANS is a very well established method for the study of polymer and colloidal samples, because it can detect inhomogeneities from around atomic scale (1 nm) to close to micron scale (600 nm), and partial deuteration can be used in order to enhance the contrast between scatterers, and between the scatterers and the solvent.

4.3.a Neutrons

SANS exploits the dual nature (wave/particle) of the neutrons. Since they have zero charge, neutrons are scattered by nuclei in samples or by the magnetic moments associated with unpaired electron spins (dipoles) in magnetic samples. Neutrons are mainly produced in two ways; continuously by a nuclear fission reactor or in pulses by spallation from a metal target bombarded by protons in a particle accelerator. Immediately after been produced the neutrons are moderated usually using liquid hydrogen in order to slow them down (make them loose kinetic energy). These neutrons are the ones used for SANS and they are called “cold neutrons”.[29]

Neutrons are scattered with the same intensity in all directions, because the wave-length of neutrons is orders of magnitude larger than the nucleus that scatters it. The main consequence of this is that in neutron scattering nuclei can be consider as “point scatterers”, which is not the case in light and X–ray scattering, where the radiation is

scattered by the electrons surrounding a nucleus (i.e. the radiation wavelength is comparable to the size of the particle).[35,36]

4.3.b SANS instrumentation

The instrumentation for SANS measurements depends on the source of the neutrons. If the neutrons come from a reactor the instrument use to measure is a fixed–wavelength or *continuous* SANS instrument. For neutrons originating in a spallation source the instrument use is of fixed geometry or *time–of–flight*.

In the fixed–wavelength instruments (as the one used in this work), a band pass filter is used in order to select a very narrow range of incident wavelengths ($\Delta\lambda/\lambda$=10-30 %). After the filter the neutrons are collimated in an evacuated flight–path, followed by the sample cell, after which the evacuated flight tube containing the detector is located. The detector is a two dimensional (area) detector which is protected from the primary neutron beam by a neutron–absorbing beam stop. A schematic representation of this kind of instruments is show in Figure 4-4.

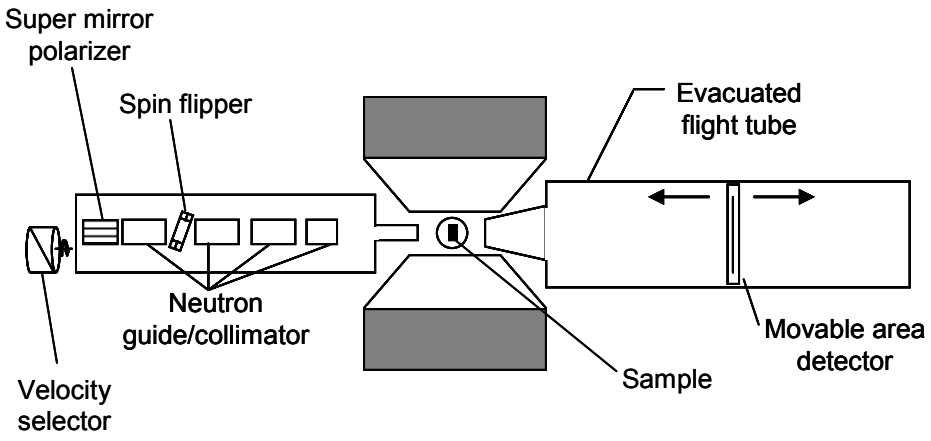

Figure 4-4. *Schematic diagram of the fixed wavelength instrument (SANS-1) at GKSS.*

The instruments used in spallation neutron sources have a fixed geometry design to allow working with a broad range of incident wavelengths in combination with time-of-flight techniques, for more details consult [29,36,37].

4.3.c Scattering length and cross section

It has already been mentioned that in SANS a two dimensional detector is used. This changes the geometry of the experiments (as observed in Figure 4-4). In a fixed–wavelength instrument once the λ has been selected, the scattering length (q) can be changed by varying the sample–detector distance (L_{sd}). For each L_{sd}, several values of the radial distance (r_{det}, corresponding to different q values) at which neutrons are recorded can be measured, see Figure 4-5.

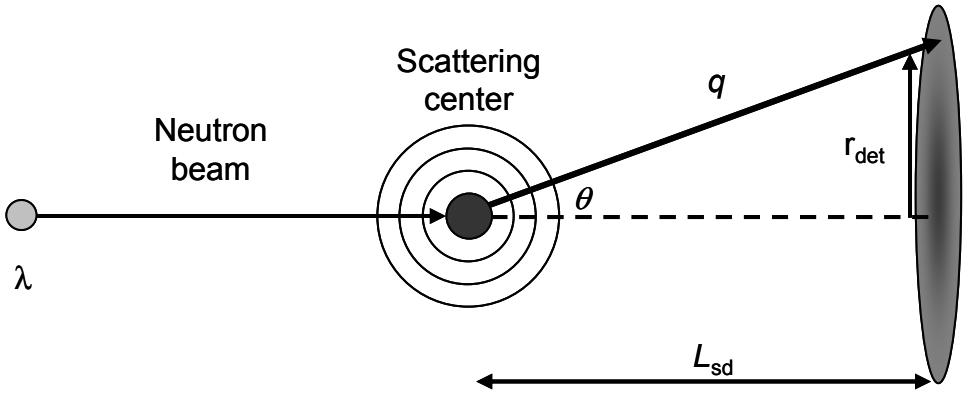

Figure 4-5. *Schematics of the geometry of SANS experiments. See text for explanations.(Adapted from [36])*

In this geometry and at small angles, a new expression for q can be derived:

$$q = \frac{4\pi n}{\lambda} sin\left(\frac{\theta}{2}\right) \approx \frac{4\pi}{\lambda}\frac{r_{det}}{L_{sd}} \tag{21}$$

By substituting this equation into the Bragg diffraction law,

$$\lambda = 2d\, sin\frac{\theta}{2} \tag{22}$$

one obtains the following expression:

$$d = \frac{2\pi}{q} \tag{23}$$

where d is the discreet distance between scattering centers, which can be determined from the position of any diffraction peak in q–space.

In neutron scattering the differential scattering cross–section $d\Sigma/d\Omega$ (q) is the dependent variable measured. It has dimensions of $(length)^{-1}$, usually cm^{-1}. This quantity is usually named intensity and is represented by the symbol $I(q)$, but this term can be misleading since in SANS what is measured is the number of neutrons at a

given wavelength, scattered through a particular angle that arrive to a small area of the detector in a unit time (flux). This flux can be expressed as:[29]

$$I(q) = I_0(\lambda)\Delta\Omega\eta(\lambda)T(\lambda)V_s \frac{d\Sigma}{d\Omega}(q) \tag{24}$$

where $I_0(\lambda)$ is the incident flux of neutrons, $\Delta\Omega$ is the solid angle element defined by the size of the detector pixel, $\eta(\lambda)$ is the detector efficiency, $T(\lambda)$ is the neutron transmission of the sample and V_s is the volume of the sample that is illuminated by the neutron beam.

The differential scattering cross–section contains information about the size, shape, and interactions between scattering centers of the sample. Thus, in general the scattering of neutrons can be expressed as:

$$\frac{d\Sigma}{d\Omega}(q) = NV^2(\Delta\rho)^2 P(q)S(q) + B_g \tag{25}$$

In this expression N is the number concentration of scattering centers, V is the volume of one scattering center, $\Delta\rho$ is the scattering length contrast (i.e. $\Delta\rho = \rho_s - \rho_m$, where ρ_s and ρ_m are the scattering length densities of solute and medium, respectively), and B_g is the background signal. $P(q)$ is the form factor (as discussed in the light scattering section) and $S(q)$ is the structure factor, which is due to interparticle interferences (it measures the interactions between particles, for dilute systems $S(q) = 1$). The term $d\Sigma/d\Omega(q)$ is also referred to as macroscopic differential scattering cross-section, in order to distinguish it form the microscopic scattering cross-section $d\sigma/d\Omega(q)$. These two terms are correlated in the following way:[28]

$$d\Sigma / d\Omega(q) = N \times d\sigma / d\Omega(q) \tag{26}$$

In neutron scattering, the sample and solvent should have different scattering length densities (ρ) in order to have some contrast (making it possible to distinguish one from the other), in the same way as in light scattering they should have different refractive index or in small-angle X-ray scattering they should have different electron density.

The scattering length densities of a molecule can be calculated using the following expression:

$$\rho = N \cdot \sum_i b_i = \frac{\delta N_A}{M} \cdot \sum_i b_i \tag{27}$$

Here δ is the bulk density of the molecule, M its molecular weight, and b_i is the coherent neutron scattering length of the nucleus i. Neutron scattering is characterized by coherent and incoherent contributions at the same time. Coherent scattering arises from the interference effects between waves scattered from different nuclei hence on the structure of the sample. By contrast, incoherent scattering is related to deviations of the scattering length from the mean value. These deviations arise not only because the scattering sample is a mixture of different isotopes, but especially because a given isotope will be found in different spin states. The neutron–nucleus interaction depeds on the total spin of the system and therefore the presence of nuclei in different spin states will cause the scattering length to vary. As the nuclear spin is usually uncorrelated with the position of the nuclei; incoherent scattering does not conatin any structural information.[38]

Of paramount importance in neutron scattering is the difference in scattering length between hydrogen (-3.741 x 10^{-15} m) and deuterium (6.671 x 10^{-15} m). This difference is the base of SANS measurements since molecules composed of light atoms (such as hydrocarbons) have a very good contrast when dissolved in deuterium oxide (D_2O). The former is the solvent preferred in this kind of measurements for its low incoherent scattering. When the scattering length contrast is equal to zero ($\Delta\rho = 0$), it is said that the solute is "contrast matched" (it has the same scattering density as the solvent). This can be achieved by replacing the hydrogen by deuterium in the molecule, or by changing the mixture of hydrogen/deuterium (water/heavy water) in the solvent. The possibility of contrast matched the solute, makes SANS measurements very suitable for work with mixtures of components (such as polymer blends, surfactant mixtures, surfactants and polyelectrolyte mixtures, among others); because it allows detecting separately the scattering from each component, permitting to see separately the conformation that each component adopts in the mixture. The values of the scattering length contrast for some of the samples used in this work are included in the appendix 1.

It should be noticed that when measuring the hydrogen activity in deuterated solutions with the usual pH cell, the values should be corrected by using the following expression:[39-41]

$$pD = 0.929\,pH \text{ meter reading} + 0.42 \qquad (28)$$

4.3.d SANS data analysis

A preliminary way of obtaining qualitative information from the neutron scattering curves is by plotting the data in a log–log form (i.e. log $I(q)$ vs. log q). These plots allow first to identify the different scattering regimes and length scales present in the sample. These scattering regimes are sample specific and can be defined as: Low–q ($q < R_g^{-1}$); Intermediate–q ($\pi R_g^{-1} < q < l^{-1}$); and High–$q$ ($l^{-1} < q$). Where "l" is the persistence length of the molecule. Different information can be extracted from the different scattering regimes. Since q^{-1} is a measurement of the length scales being studied, in the low–q regime one is studying large length scales, corresponding approximately to the dimensions of a polymer or polymer aggregate; at intermediate–q, the excluded volume effects dominate the polymer conformation; and high–q, short length scales, correspond to polymer segments.

Table 4-1. *Fractal dimension exponents of selected systems.*[36]

Systems	D_f
Rod–like chains	-1.00
Gaussian chains in good solvent	-1.66
2D network	-1.90
Gaussian chain in theta solvent, lamellar, platelet, and disk structures	-2.00
Randomly branched Gaussian chain	-2.28
Weakly segregated 3D–networks	-2.50
Volume fractals	-3.00
Bodies with smooth interfaces such as spheres and strongly segregated 3D–networks	-4.00

The log $I(q)$–log q plot, can also help to determine the fractal dimensions (D_f) of the molecules in solution, which can be correlated to different structural conformations. The fractal dimensions can be calculated from the slope of the scattering curve (in the linear parts at intermediate and low q regimes). Since:

$$\frac{d\Sigma}{d\Omega}(q) = NV^2\Delta\rho^2 q^{-D_f} \tag{29}$$

Different values of D_f corresponding to different conformations are listed in Table 4-1.

There are a relatively large variety of ways for plotting the scattering data in order to obtain information (generally M and R_g) about the system at the different scattering regimes. Some of these graphs can only be applied on the low q–range, and can be used to analyze static light scattering data as well. A summary of the different plots can be found in [36].

A more complete analysis of small–angle scattering data can be done following two different approaches; model independent or direct modeling. The model independent method developed by Glatter,[42,43] provides information about the distribution of the scattering units (pair distribution function) *p(r)* by applying the Indirect Fourier Transformation Method (IFT). When this method is applied over the entire q–range one obtains information about the whole structure of the aggregates, whereas if it is applied at high q–values one obtains information about the local structure within the aggregate, such as its cross section. Once the analysis of the *p(r)* has been done it may be possible to develop an analytical model that can be fitted to the data.[44]

For direct modeling of the data, a detailed structural model of the aggregates is invoked and a scattering curve is generated, then the calculated scattering curve is compared with the experimental data. One has to be aware that more than one model can describe a specific scattering curve; additional information about the system is thus necessary in order to select which model is most likely to be correct. A description of the fitting procedure as well as a complete summary of the different form and structure factors for several different conformations can be found in [44].

4.4 SLS in "neutron units"

It has already been established that complementary information at different q–ranges can be obtained from both static light scattering and small-angle neutron scattering. In some systems one can benefit from the information obtained by both techniques, e.g., while performing model fitting of the data in systems that are larger than the largest length scale measured by SANS. However, before doing any data processing it is necessary to bring all the data to the same intensity scale.

The SLS data can be converted into "neutron scattering units" by multiplying it with the following factor:

$$\frac{K_C}{K} \cdot \frac{(\Delta\rho)}{N_A} \tag{30}$$

where:[45]

$$K_C = \frac{R_k}{I_{tol}} \left(\frac{n}{n_{tol}} \right) \tag{31}$$

is the correction factor for the instrument geometry, with R_k the Rayleigh ratio for the calibration medium (toluene), I_{tol} is the scattering intensity of toluene, n and n_{tol} the refractive index of the solvent and toluene at the wavelength of the instrument, respectively. K is the optical constant for vertically polarized incident light (equation 4), and $\Delta\rho$ is the scattering length contrast per unit mass.

If the sample that is been analyzed is a mixture of solutes, then $\Delta\rho$ is calculated as follows:[46]

$$\Delta\rho = \sum_i X_i \Delta\rho_i \tag{32}$$

where X_i is the mass fraction of the component i and $\Delta\rho_i$ is its scattering length contrast.

5 MATERIALS

5.1 Surfactants

Different kinds of surfactants (anionic and nonionic) were used in this work. For a list of the surfactants and their critical aggregation concentration (cmc) in pure water, see Table 5-1.

Table 5-1. *Summary of the surfactants employed in this work, their abbreviations and their critical aggregation concentration (cmc) in pure water at 25 ℃.*

Type	Surfactant name	cmc (mM)
anionic	Sodium dodecyl sulfate (SDS)[1,47]	8.3
	Sodium decyl sulfate[1,47]	33.0
	Sodium octyl sulfate[1,47]	133.0
nonionic	Penta(oxyethylene) dodecyl ether ($C_{12}E_5$)[48]	0.064
	n-dodecyl β-D-maltopyranoside (C_{12}-mal)[49]	0.167
	n-decyl β-D-glucopyranoside ($C_{10}G_1$)[50]	2.2

5.2 Polyelectrolytes

5.2.a Mucins

Mucins are glycoproteins containing a large number of oligosaccharides (between 70-90% of the molecule) that are covalently bound to a protein backbone (which accounts most of the remaining 10-30% of the molecule). Most of the carbohydrate side–chains are confined to certain regions that alternate with less densely populated areas were the protein backbone is exposed. Mucin subunits are held together by disulfide bonds, forming large molecules with molecular weights in the order of millions.[51,52] Mucins are produced by glands in the submucosal connective tissue or

by secretory cells in the surface epithelium. They are responsible for the properties of the mucus that covers most of the epithelial surfaces, protecting them from the outside word.[53,54] The high amount of oligosaccharide side chains, which can contain from 30-40 glycan units in a linear or branched configuration, allows mucin to interact strongly with water. This explains how mucus is formed by around 90% water and only 0.5-5% mucin, while proteins originated from the underlaying tissue and from the interstitial fluid account for the rest of the mucus.[51,55] The net negative charge of mucins is due to the fact that at least half of the oligosaccharides in mucin carry acidic groups in the molecule.[55,56]

In this work bovine submaxillary mucin was studied as receive from the provider without further purification

5.2.b Polyethylene imine (PEI)

PEI is a hyperbranched polyelectrolyte composed of primary secondary and tertiary amine groups in a ratio of 1:2:1.[57,58] The charge of this polyelectrolyte can be regulated by adjusting the pH of the medium where it is dissolved.[59] Due to the conformation of the polyelectrolyte the maximum amount of amine groups that can become charged is around 70%.[57,59,60] A representation of the structural element of a PEI monomer can be seen in Figure 5-1.

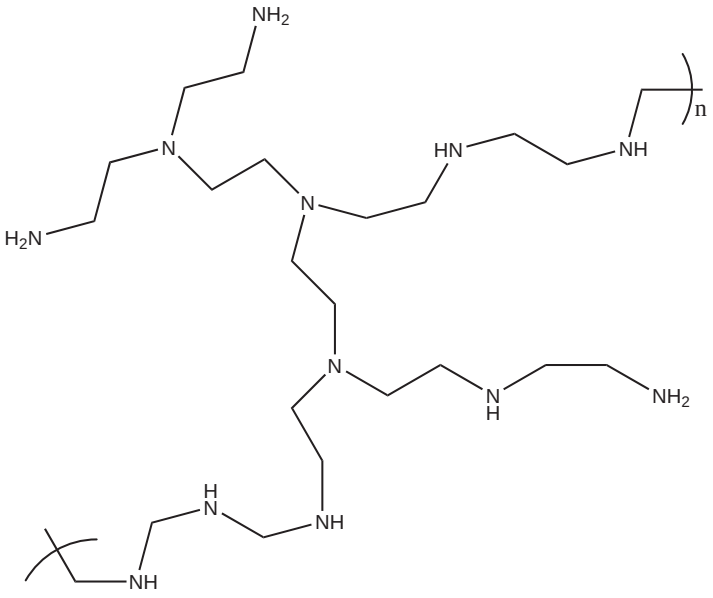

Figure 5-1. *Structural element of polyethylene imine.*

5.2.c PEO$_{45}$MEMA:METAC-2

Poly(ethylene oxide) monomethylether methacrylate and methacryloxyethyl trimethylammonium chloride (PEO$_{45}$MEMA:METAC-2) is a comb polyelectrolyte resulting of the free radical polymerization of poly(ethylene oxide)-2000 methyl ether methacrylate (PEOMEMA) and methacryloxyethyl trimethylammonium chloride (METAC). In this polyelectrolyte 2 mol% of the methacrylate units carry a permanent charge while the other 98 mol% a 45 unit long PEO side-chain.[61] Figure 5-2 shows the structure of PEO$_{45}$MEMA:METAC-2.

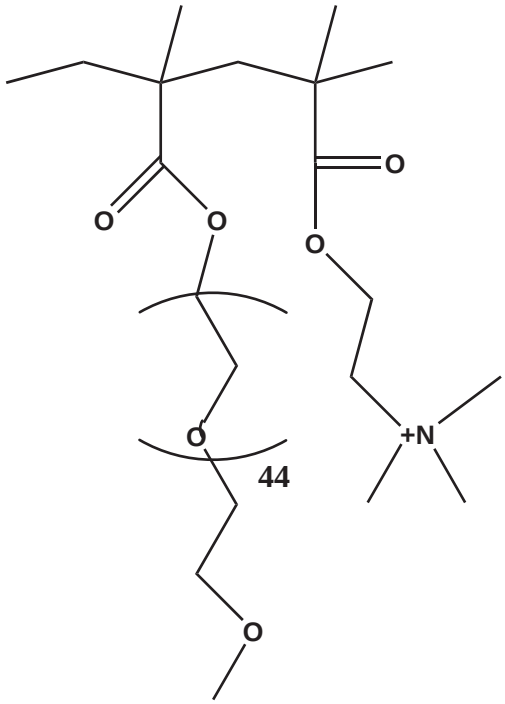

Figure 5-2. *Structure of PEO$_{45}$MEMA:METAC-2 monomer units.*

5.2.d Chitosan

The product of the alkaline or enzymatic deacetylation of chitin results in chitosan, a copolymer of D-glucosamine and β(1-4) *N*-acetyl-D-glucosamine. High molecular weight chitin, a copolymer of β-D (1-4) *N*-acetyl-D-glucosamine, is second to cellulose as the most abundant biopolymer in nature. It can be found in the exoskeleton of crustaceans, invertebrates, insects, and in the cell wall of fungi and yeast. The pKa of chitosan is around 6, therefore chitosan behaves as a highly charged

polyelectrolyte at low pH values.[62-65] While chitin is basically non soluble in aqueous solution, chitosan is soluble in weakly acidic solutions.[65,66] A structural unit of chitosan can be observed in Figure 5-3.

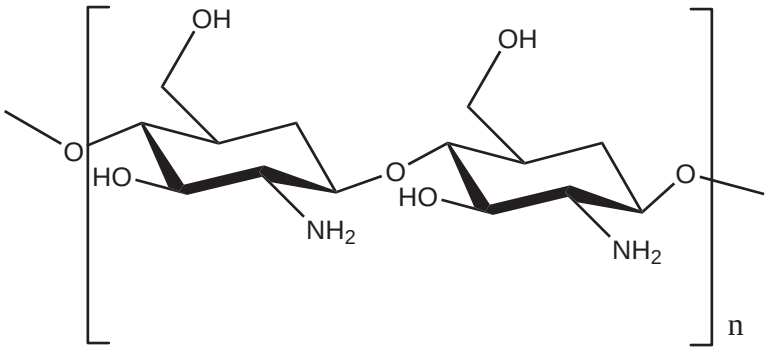

Figure 5-3. *Chemical structure of chitosan*

6 METHODS

The results presented in this work were obtained by using several experimental techniques. From the point of view of the present investigation the measuring principle, information obtained and limitations of each technique are summarized in the table below. More details about the techniques can be found in the articles and the references included in the table.

<table>
<tr><th>Measuring Principle</th><th>Information Obtained</th><th>Limitations</th></tr>
<tr><td colspan="3">Dynamic Light Scattering[21,67,68]</td></tr>
<tr><td>A laser beam is directed towards the sample, the variation of the intensity of the scattered light with time is measured.</td><td>Random motion of particles in solution. (Translational Diffusion coefficient).
Hydrodynamic radius.</td><td rowspan="3">Solvent should have different refractive index than solute.
Results can be affected by small fraction of aggregated species or dust.
Opaque samples can not be measured. Typical length scales probed: 10-5000 nm.</td></tr>
<tr><td colspan="2">Static Light Scattering[21,31,67,68]</td></tr>
<tr><td>As in dynamic, but the variation of the time–average intensity of the scattered light as a function of the scattering angle is measured.</td><td>Molecular weight, mean square radius of gyration, second virial coefficient.</td></tr>
<tr><td colspan="3">Reflectometry[69]</td></tr>
<tr><td>A laser beam is directed towards the surface at close to the Brewster angle*. Intensities of the normal & parallel polarizations of the reflected beam are measured.</td><td>Adsorbed amount per unit area.
Kinetic information of the adsorption process in a well define geometry.</td><td>Insensitive to the concentration profile of the adsorbed layer.
Refractive index of adsorbed film and solvent should be different, and known.</td></tr>
<tr><td colspan="3">Surface Tension[1,31,70,71]</td></tr>
<tr><td>Wilhelmy plate method: Measures the weight (drag force) of the meniscus formed around the plate.</td><td>Surface tension.</td><td>The contact angle between the liquid and the Wilhelmy plate should be known.</td></tr>
</table>

* i.e. the angle where the reflectivity parallel to the plane of incidence is zero.

Small-Angle Neutron Scattering (SANS)[29,36]		
Cold neutrons are directed to the sample. The variation of the neutrons scattered intensity at different sample to detector distances is measured.	Radius of gyration, correlation length, persistence length, etc. More detail structural information by model fitting of the data.	Limited use in time dependent processes. The necessity to use model fits which are usually not unique. Typical length scales probed: 0.5-600nm. Limited access to beam time.
X-Ray Diffraction[32,36,72]		
Samples with periodic structures cause an incident beam of X-rays to interfere with one another as they leave the sample.	Morphology and dimensions of structured domains in the sample. Degree of alignment and orientation.	Very thin samples (i.e. thin films, or small volumes). Radiation can damage some samples. Typical length scales probed: 0.1-2500nm.
Electrophoretic Mobility[31]		
Movement of particles under the influence of an electric field.	Diffusion of particles, the Zeta potential is calculated.	Shape of aggregates should be known to determine the charge and Zeta potential.
Nuclear Magnetic Resonance (NMR)[32,73]		
Transitions between energy levels of some nuclei in a magnetic field.	Adsorption of radio-frequency energy vs. magnetic field. Diffusion.	Average signals from measurements, some species can be overlapped by other signals.
Atomic Force Microscope (AFM)[70,74,75]		
Measures short range inter-atomic forces between a sharp probe and a surface.	Surface forces and imaging of samples.	Cannot measure thickness of the adsorbed layer on the samples.
Potentiometric titration[76,77]		
Measures the potential as a function of the ionic activity of a solution.	The concentration of free ions in solution.	Only acidic and basic sites of certain strength can be detected. Hydrogen ion gradient in colloidal solutions.

7 RESULTS AND DISCUSSION

7.1 Mucin and Sodium Alkyl Sulfate Surfactants

7.1.a Interactions in bulk

The dissolution of mucin in aqueous solution (30 mM NaCl) results in complex DLS curves with two distinctive peaks at different relaxation times. The two peaks were observed at different mucin concentrations (from 5 ppm to 100 ppm). The peak of a freshly prepared 25 ppm mucin solution corresponds to a hydrodynamic radius (R_H) of 720 nm with a shoulder corresponding to 160 nm. The scattering curves were dominated by the larger species, but in fact the mass fraction of the small and large species, determined by the normalized area below each peak, was roughly the same.

Static light scattering (SLS) measurements gave a radius of gyration (R_g) of around 820 nm for the large species and the molecular weight could not be determined. From these measurements it was concluded that the large species in the mucin solutions corresponded to aggregates of several mucin molecules. The ratio R_g/R_H was 1.6 corresponding to a random coil conformation.[78]

Next, the effect of sodium dodecyl sulfate (SDS) on the mucin aggregates in solution (30 mM of NaCl), was investigated. At low concentrations SDS has very small effect on the mucin aggregates (Figure 7-1). When a critical surfactant concentration is reached (0.75 mM SDS ≈ 0.2 cmc) the aggregate size starts to decrease, a further increment of the surfactant concentration results in a significant change in the mucin aggregates, see Figure 7-1.

The disaggregating process of mucin aggregates was found to be time dependent. At concentrations below 0.2 cmc SDS the size of the mucin aggregates did not change significantly even after 48 hours of preparing the solution. At 0.2 cmc SDS the deaggregation time was long (more than 13 hours). While at higher surfactant concentrations the kinetics of the disaggregating process were faster (just a couple of hours).

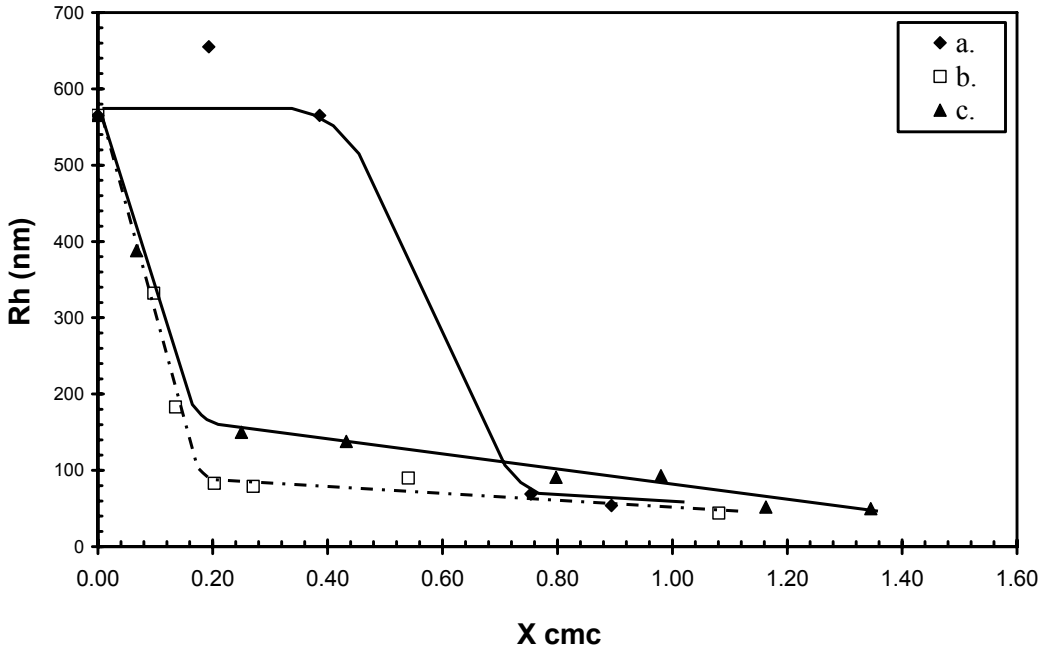

Figure 7-1. *Hydrodynamic radius for mucin/sodium alkyl sulfate aggregates. Aged solutions (48 h). All of the solutions contained mucins (25ppm) and NaCl (30mM).* **a.** *Sodium octyl sulfate.* **b.** *Sodium decyl sulfate.* **c.** *Sodium dodecyl sulfate.*

Since both mucin and sodium alkyl sulfate surfactants have the same charge in solution, the interaction between these two kinds of molecules is most likely promoted by hydrophobic interactions between the tails of the surfactants and the protein backbone. In order to test this hypothesis, sodium alkyl sulfates with chain lengths shorter than SDS, were added to mucin solutions (25ppm and 30 mM NaCl). A lower concentration of SDS, compared to sodium decyl sulfate, was required to dissolve the mucin aggregates. However, when the concentration of the surfactants was normalized to their cmc (see Figure 7-1), one finds that the deaggregation occurs at the same fraction of the cmc (0.2 cmc) for both surfactants. This is a slightly lower concentration than the critical aggregation concentration, cac, of SDS with poly(ethylene oxide), about 0.5 cmc,[79,80] but higher than that between SDS and cataionic polyelectrolytes.[81] Sodium octyl sulfate was not as effective as the longer chain surfactants, since a higher concentration of this surfactant (around 0.5 cmc) was required to see any effect. Therefore, the surfactant alkyl chain has to be long enough

to promote deaggregation, supporting the hypothesis that hydrophobic interactions are important for the association process.

The change in ionic strength affects the association of SDS to mucin, in the same way as it affects the cmc of the surfactant. Higher amounts of surfactant were required in order to start the deaggregation process at low ionic strength (1 mM NaCl), while lower amounts of surfactant were required at high ionic strength (100 mM NaCl). This can be explained by the screening of electrostatic interactions promoted by the presence of electrolyte between the charged surfactant head groups and the charged proteins.

7.1.b Interactions at interfaces

The surface tension isotherm of SDS with and without added mucin (25ppm) in 30 mM NaCl can be observed in Figure 7-2a. Mucin aggregates are surface active, the surface tension of pure mucin solution was found to be around 65 mN/m. Addition of SDS to the mucin solution results in a further decrease in the surface tension (to around 45 mN/m), which indicates that the mucin/SDS aggregates are more surface active than either of the components by themselves. The values of the surface tension remain below the values for the pure surfactant up to its cmc. After this point the values of the surface tension of the mucin/SDS solution are the same as the ones for the pure surfactant.

Reflectometry measurements showed that BMS adsorb to both hydrophobic and hydrophilic silica. SDS is very effective in removing pre-adsorbed layers of BSM from silica and to a lesser extent on hydrophobized silica (for more details, see Paper II).

7.2 Mucin and nonionic surfactants

7.2.a Interactions in bulk

DLS measurements were performed on mucin (25 ppm) in 30 mM NaCl and in presence of the nonionic surfactants $C_{12}E_5$ and C_{12}-mal (at their respective cmc values). The addition of the mentioned surfactants to the mucin solution has no significant effect on the mucin aggregate size even after 48 hours.

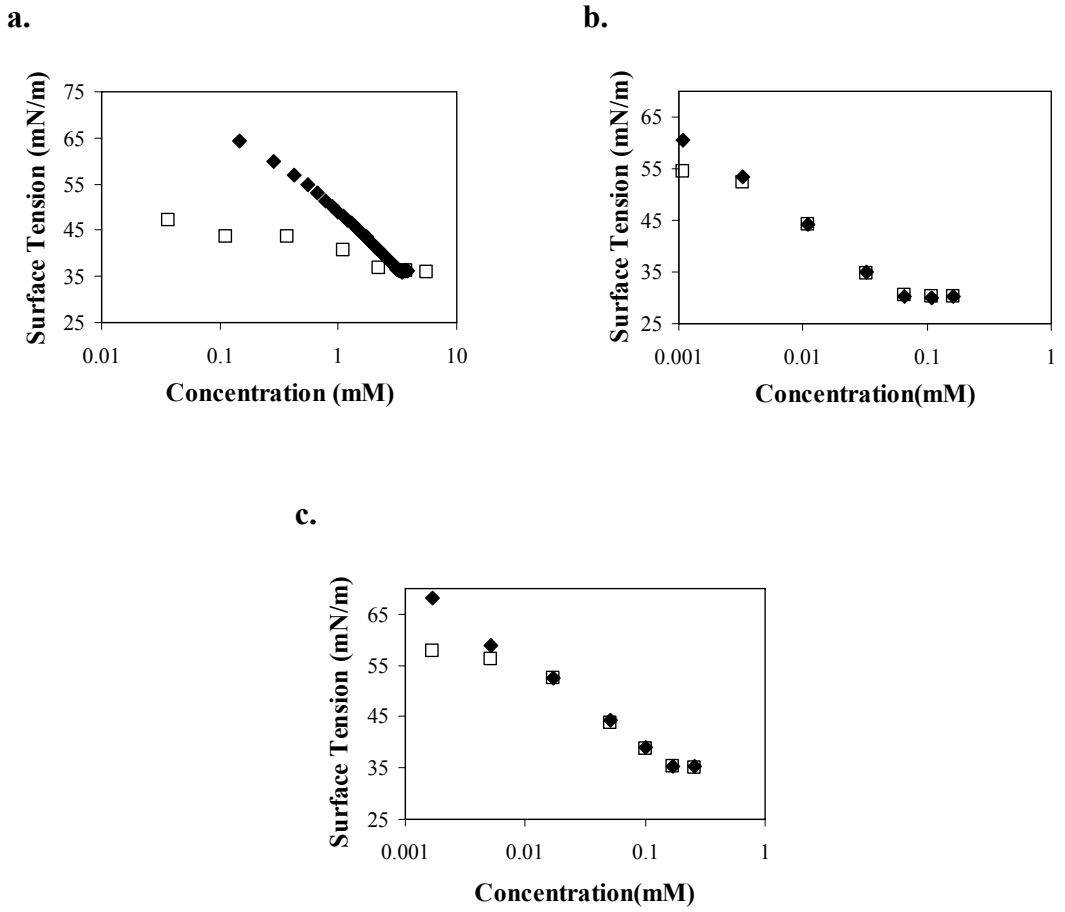

Figure 7-2.**a.** *Surface tension isotherm for SDS in 30 mM NaCl with (□) and without (♦) 25 ppm BSM.* **b.** *Surface tension isotherm of $C_{12}E_5$ in 30 mM NaCl with (□) and without (♦) 25 ppm BSM.* **c.** *Surface tension isotherm of C_{12}-mal in 30 mM NaCl with (□) and without (♦) 25 ppm BSM. All measurements where done after equilibrating the solutions for 48 hours.*

7.2.b Interactions at interfaces

The lack of any dramatic effect of the $C_{12}E_5$ and C_{12}-mal on the mucin aggregate size can not be interpreted as a lack of interaction between these molecules. In order to verify if these nonionic surfactants associate or not with mucin, surface tension isotherms of pure surfactant and surfactant–mucin solutions were obtained (Figure 7-2). The addition of low amounts of both $C_{12}E_5$ and C_{12}-mal to mucin solutions, results in a lowering of the surface tension values below the value obtained for the pure BSM. A further increment in the surfactant concentration has as a consequence that the surface tension values returned to the values of the pure surfactant solutions

(Figure 7-2b and c). This is a clear indication that the surfactant has displaced the mucin aggregates from the interface, and that if there is any surfactant adsorption to the BSM it is not a large amount.

7.3 Structures of Polyethylene Imine / SDS complexes in D_2O

It has been shown how the hydrophobic interactions overcome the electrostatic ones, resulting in association between the negatively charged sodium alkyl sulfates and mucins in aqueous solution. Random coil mucins decorated with SDS was the model proposed to describe these aggregates (Figure 8-1, section 8). Stronger interactions are then expected for the case when oppositely charged surfactants and polyelectrolytes are mixed in solution. The interactions between the hyperbranched cationic polyethylene imine (2000 ppm) and SDS were studied at two different pH values (polyelectrolyte charge densities) with SANS and light scattering using D_2O as a solvent.

7.3.a Polyethylene imine mixed with SDS at pD 10.1

At these conditions PEI is weakly charged, and no precipitation of the sample was observed at any surfactant concentration studied. The static light scattering curves of these samples were rather similar (Figure 7-3) and their intensity increased with the surfactant concentration up to the highest SDS concentration investigated (16.6 mM).
Similar observations can be made on the SANS curves (for protonated SDS, *h*–SDS), where the addition of even small amounts of surfactant results in an increment of their intensity. The shape of the SANS curves is rather complex, especially at high surfactant concentrations, where different slopes are observed at different q ranges, see Figure 7-3. This behavior contrasts significantly with the one observed in the scattering curves for deuterated SDS (see Paper III), where the addition of surfactant causes very small changes on the intensity and shape of the curves, thus reveling that the surfactant addition does not result in large conformational changes on the polyelectrolyte.
From these observations it was proposed that the surfactant adsorbs on a PEI template. Detailed information about the conformation of the PEI and PEI–SDS aggregates was obtained by model fitting the static light scattering and SANS data (solid lines in Figure 7-3). With no or low surfactant concentrations the scattering curves could be fitted with an elongated ellipsoid model (with half axes of 1100 x 55

x 7 Å). At and above 2 mM of SDS, these ellipsoidal aggregates start to stack on top of each other. The distance between these stacked ellipsoids decreases as the surfactant concentration increases, probably due to a decreased electrostatic repulsion and increased attraction between surfactant tails on neighboring ellipsoidal objects in the stacked structure. The stacking is, however, rather disordered (see Figure 8-2a, Section 8).

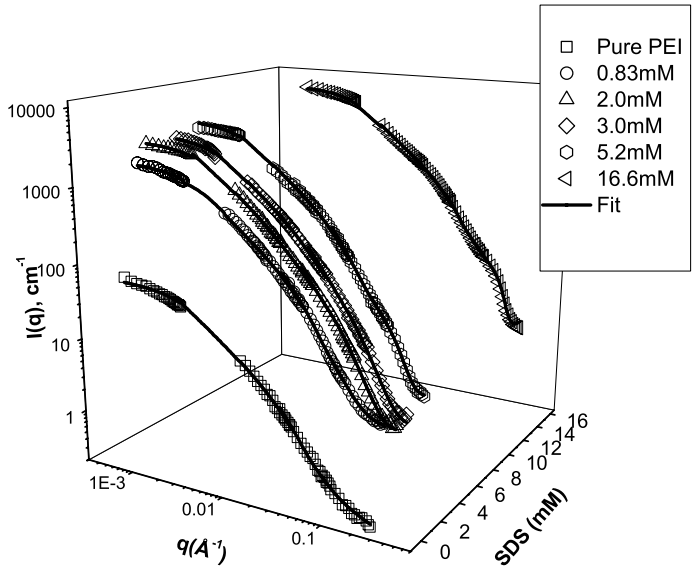

Figure 7-3. *Scattering data for PEI samples (2000 ppm) at pD 10.1 and different h-SDS concentration in D_2O obtained by SANS (high q–values) and SLS (low q–values). The legends to the right show the h-SDS concentration in the samples. The solid lines are calculated scattering curves obtained by using the Paracrystal ellipsoidal bilayers model described in the text.*

7.3.b Polyethylene imine mixed with SDS at pD 4.9

At this pD value the degree of ionization of PEI is around 69%.[57] The samples were too turbid to allow static light scattering measurements, even at the lowest surfactant concentration studied (0.83 mM SDS), which shows that large surfactant/polyelectrolyte aggregates were present in solution[82,83] already at this low surfactant concentration. At higher surfactant concentrations the aggregates

precipitate and they do not redissolve again even at the highest surfactant concentration studied (232 mM).

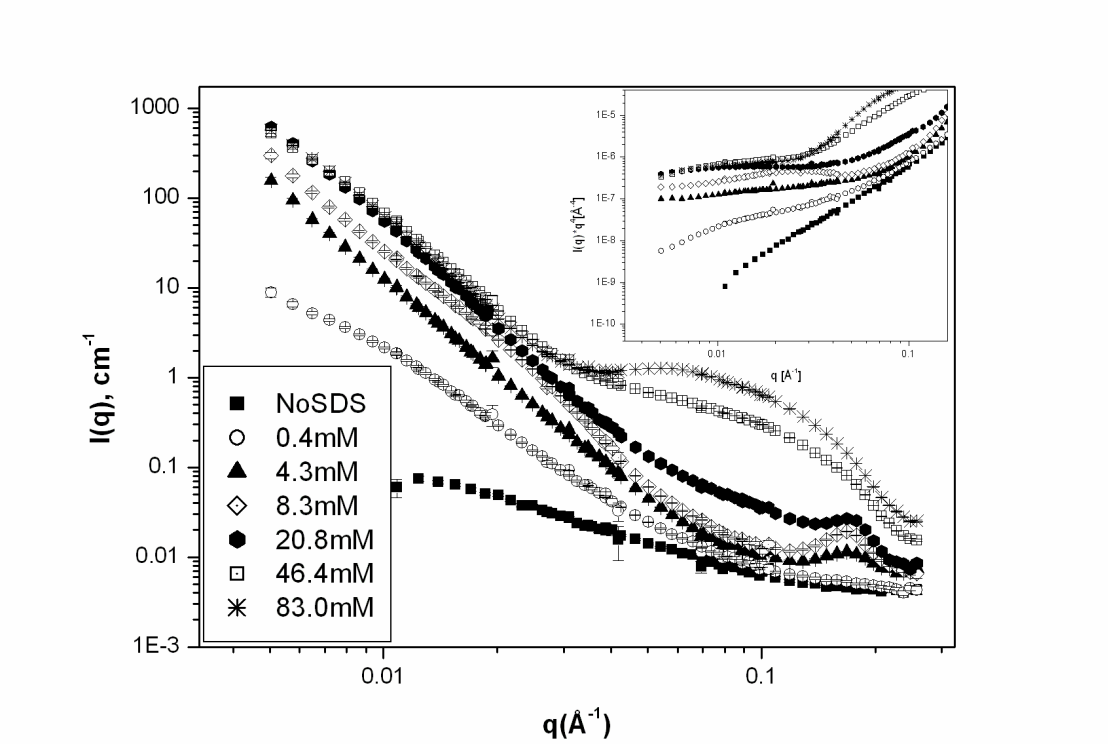

Figure 7-4. *SANS data for PEI samples (2000 ppm) at pD 4.9 and different SDS-h concentrations in D2O. The legends to the left show the SDS-h concentration in the samples. The inset shows a plot of $I(q)q^4$ as a function of q. At high SDS concentrations the value of Iq^4 becomes close to constant at low q values, which is indicative of the presence of large aggregates with smooth interfaces.*

SANS data show that even the addition of small amounts of *h*–SDS results in a considerable change in the scattering curve, see Figure 7-4. At low surfactant concentrations (up to 0.4 mM), the slope of the curve at intermediate *q*–values is q^{-2}, corresponding to disk like aggregates.[36] As the SDS concentration is increased the slope of the curves at the same *q*–values changes to q^{-4}, which corresponds to the formation of large three–dimensional aggregates with smooth interfaces. These aggregates have an ordered internal structure as evidenced by the Bragg–like peak at *q*

= 0.17 $Å^{-1}$ (in the SDS concentration interval 4.3–20.8 mM), which corresponds to a repeat distance of 37 Å. The intensity of the peak increases with surfactant concentration, while it stays in the same position, which is an indication that more polyelectrolytes/surfactant aggregates adopted the same structure. At higher surfactant concentrations (above 20.8 mM SDS), the Bragg–like peak is overlapped by a broader peak probably due to the presence of free surfactant micelles. By studying the precipitate from the sample at 46.6 mM SDS using X–ray diffraction, it was confirmed that there was still an ordered structure in the aggregates, even in the presence of free surfactant micelles, and that these aggregates have a lamellar conformation with a repeat distance of 37 Å (Figure 8-2b, Section 8). Similar values of repeat distances had been reported for polyvinyl amine with SDS and other alkyl sulfates.[8,84]

It has be shown thus, how PEI/SDS aggregates change their conformation from stacked aggregates with poorly defined repeat distance to highly organized lamellar structure, by increasing the charge density of the polyelectrolyte via decreasing the pD value.

7.4 Deuterium isotope effects on the PEI/SDS interaction

Solvent isotope effects have been observed in different systems like biological,[85] surfactants,[86,87] surfactant mixtures,[88] and different polyelectrolytes.[89,90] It has been shown in the previous section, how sensitive PEI is to the solvent composition (pH). In this section the effect of the isotopic substitution of H_2O with D_2O on the interactions between SDS and PEI is discussed.

The PEI/SDS samples were investigated at three pH/pD values, at the natural pH of the PEI samples, at pH/pD around 9 and at pH/pD = 4.

The values of the pD of the pure PEI samples in D_2O are around 0.8 units higher than the pH values in water. Since the charge density of PEI depends on the pH of the solvent, this seems to indicate that the charge density of PEI is higher in D_2O than in H_2O in this pH range. However, as shown in Figure 7-5a, the molecule has an equally low charge density in both solvents.

One of the most important features of Figure 7-5a is that PEI/SDS complexes reach the point of zero mobility (charge neutralization point) at the same surfactant concentration (1.5 mM SDS), in both solvents. Overall, the electrophoretic mobility values in D_2O are lower than in H_2O, but if the 20 % higher viscosity of D_2O is taken

into account (dotted line in the figure), it becomes evident that the differences in mobility between the two samples are minimal.

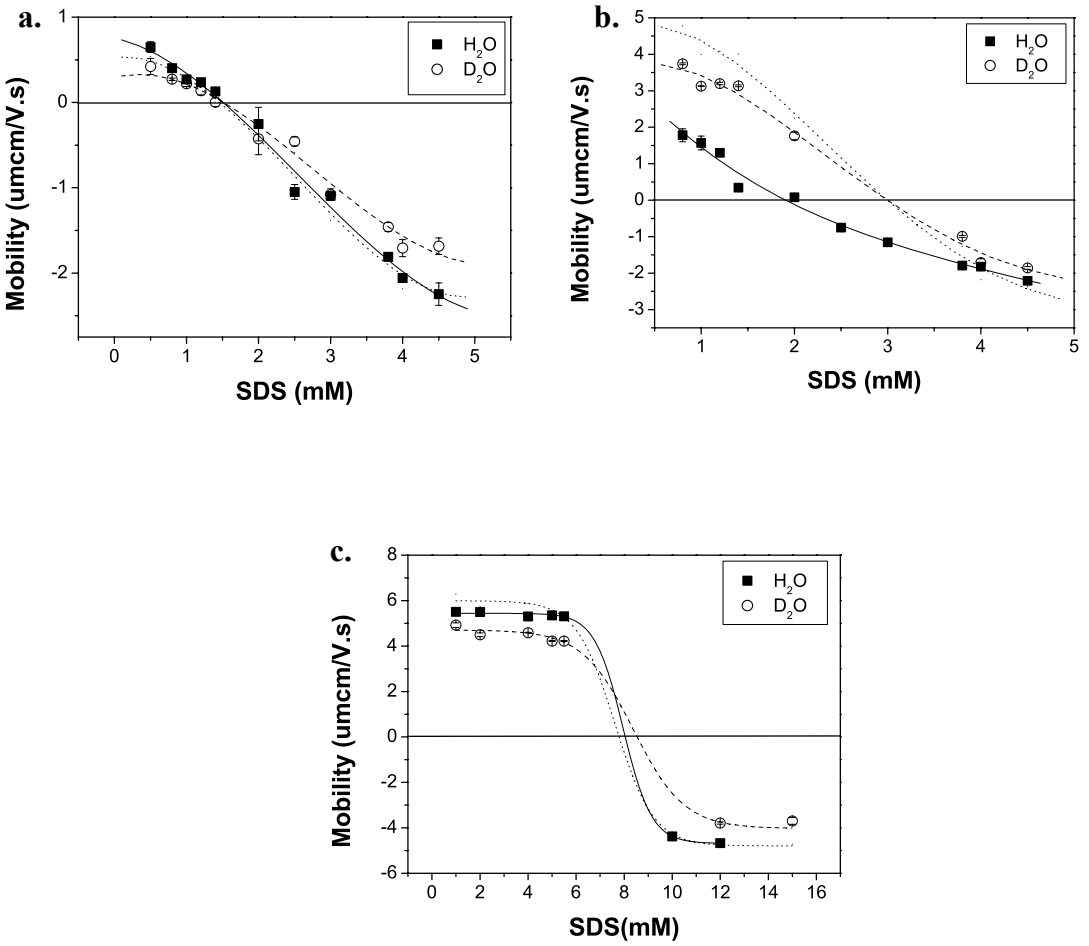

Figure 7-5. *Electrophoretic mobility of PEI/SDS aggregates as a function of SDS concentration, in two different solvents, as indicated on the legend on the right-hand sight of the figure. The measurements were done at* ***a.*** *The natural pH of the samples,* ***b.*** *At pH = 8.8 and pD = 8.5, and* ***c.*** *At pH/pD = 4.0. The PEI concentration was 0.05%. The points shown are average values of five measurements, whereas the solid and dashed lines are guides for the eyes. The dotted line illustrates the viscosity corrected mobility data obtained for the samples in D_2O.*

The differences in viscosity between the two solvents can not explain the differences observed between the samples of PEI/SDS dissolved in water and heavy water at

pH/pD around 9. As seen in Figure 7-5b, the electrophoretic mobility values in D_2O at low surfactant concentrations are almost double the values in H_2O. If the correction for the viscosity of heavy water is taken into account these differences are enhanced. Moreover, the charge neutralization point in D_2O (3.1 mM SDS) is higher than the one in H_2O (2 mM). These results agree with the potentiometric measurements done on pure PEI in H_2O and D_2O (see Paper IV)[91], which show that PEI has a significantly higher charge in heavy water than in water at this pH range.

For the case of PEI at pH/pD = 4, similar high charge densities for the samples in both solvents were observed (Figure 7-5c), which is in good agreement with the pontetiometric titration. The charge neutralization point was the same for both samples.

In conclusion, great care must be taken when analyzing experiments in which weakly charged polyelectrolytes are investigated in heavy water, and then correlating the observations made with the same system in water.

7.5 Micelles formed in aqueous mixtures of a nonionic alkylglucoside and an anionic surfactant

Very large isotopic solvent effects were also observed when studying mixtures of *n*-decyl β-D-glucopyranoside ($C_{10}G_1$) and SDS. Static light scattering measurements indicated that when these surfactants are mixed at [SDS]/[$C_{10}G_1$] = 1:3; and [NaCl] = 100 mM, the micelles formed in D_2O are five times larger than the micelles formed by the same samples in water. Previous reports on isotopic effects on the size of micelles formed by sugar–based surfactants, attributed the difference in micellar size between the two solvents (i.e. water and heavy water) to an increased hydrophobicity in D_2O.[86,87] In this case the increase of the micellar size was linked to a considerable decreased of the cmc of the system, indicating an increase in hydrophobicity of $C_{10}G_1$ in D_2O compared to H_2O.

SANS measurements, on the other hand, indicated that the size and shape of these mixed surfactant micelles were strongly dependent on their composition (i.e. the fraction of each surfactant present in solution), the overall surfactant concentration, and the ionic strength of the solutions. At low ionic strength (0 and 10 mM NaCl), the scattering data was best fitted with a model corresponding to prolate ellipsoids of revolution. In Figure 7-6, it can be seen how the short half axis size (*a*), remains

constant while increasing the mole fraction of SDS in the sample (at 0 mM NaCl). However, the long half axis size (*b*) decreases with increasing the mole fraction of SDS. For the samples at 10 mM NaCl the same trend was observed, with the difference that the large half axis of the micelles formed at [SDS]/[$C_{10}G_1$] = 0.25 were around 1.3 to 1.7 times larger than the ones formed at 0 mM NaCl.

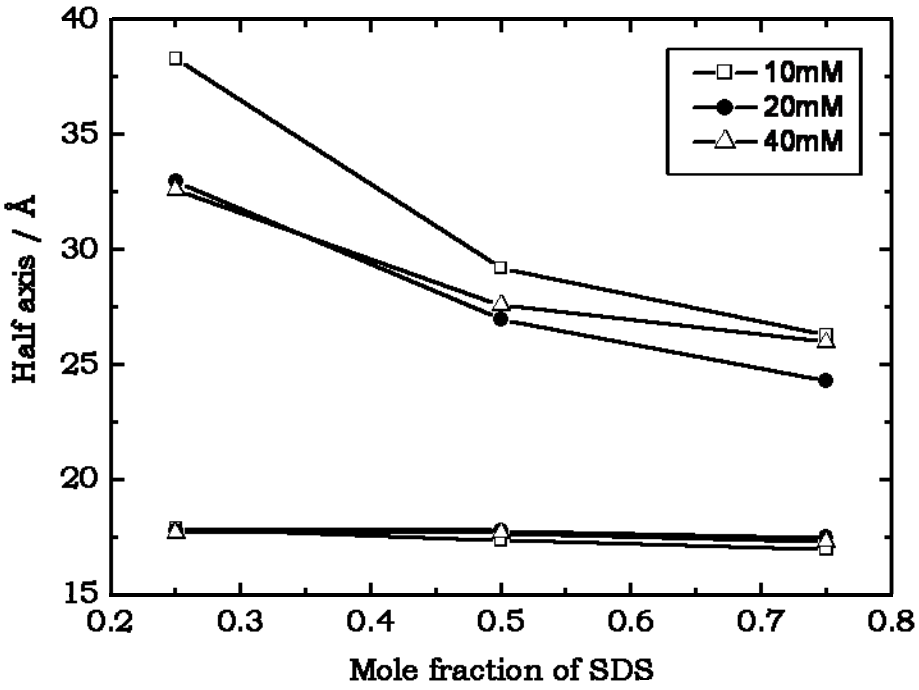

Figure 7-6. *Half axes "a" (lower symbols) and "b" (upper symbols) of mixed SDS/ $C_{10}G_1$ micelles formed in the absence of added salt plotted against the mole fraction of SDS, x = [SDS]/([SDS]+[$C_{10}G_1$]). The overall surfactant concentrations are shown in the legend to the right of the figure.*

These ellipsoids grow considerably in length when the electrolyte concentration is increased to 100 mM NaCl. Here, rigid rods appear at surfactant compositions of [SDS]/[$C_{10}G_1$] = 3:1 and 1:1, whereas very long flexible worm like micelles were observed when the alkylglucoside was present in excess i.e. [SDS]/[$C_{10}G_1$] = 1:3. It was in the latter samples that the isotopic effects were observed.

7.6 Complexes of low charge density comb polyelectrolytes and SDS

In sections 7.3 and 7.4, it was shown how mixtures of oppositely charged surfactants and polyelectrolytes result in phase separation under certain conditions. A way around this is the incorporation of poly(ethylene oxide) (PEO) into the polyelectrolyte structure.[60,83,92]

The scattering curves of pure PEO_{45}MEMA:METAC-2 (0.2%) in D_2O and at SDS concentrations up to 2 mM, present a slope of q^{-1} at q–values of $0.005 < q < 0.025$ Å^{-1}, which is characteristic of rod like structures (see Figure 7-7). For the sample at 8 mM SDS, in the same q–range, the slope is $q^{-0.9}$. This reduction of the slope is an indication of repulsive interactions between the aggregates. At intermediate q–values ($0.025 < q < 0.09$ Å^{-1}) for samples containing up to 2 mM SDS, the slope is proportional to q^{-4}, which is indicative of a smooth interface between the scattering object and the surrounding solution. At the same q–range, this slope changes to $q^{-2.7}$ for samples at SDS concentrations of 4–8 mM. Therefore, the cross-section interface of these rods with the solvent becomes less define as the total SDS concentration is increased above 2 mM SDS.

In Figure 7-7 it can be observed how the incorporation of a small amount of surfactant, determined by NMR to be 0.2 mM at a total surfactant concentration of 4mM, has a significant impact on the structure of the complex.

A model based on “stiff rods with elliptical cross section” was chosen in order to analyze the scattering data. The scattering curve calculated with that model was very similar to the experimental data of the samples at surfactant concentrations up to 2 mM, over the whole q–range (see solid lines in Figure 7-7). The calculated half axes of the elliptical cross section of the rods were 41 and 79 Å for these samples.

At SDS concentrations of 4 mM and higher, the stiff rod elliptical cross section model could not be used to explain the data. The data was instead well described with a core–shell rod–like model. The outer shell was equal to 56–59 Å, and the inner shell radius was equal to 16 Å. The significant lower scattering length density of the outer shell compared to the inner one seems to indicate that the shell consists of a mixture of SDS associated with the polyelectrolyte backbone and parts of the PEO side chains; whereas the outer shell consists of PEO chains that are forced to extend further away from the backbone due to the presence of SDS within the aggregate (see Figure 8-3b,

section 8). Similar structures have been proposed for comb like copolymer–surfactant complexes, with shorter PEO chains.[93,94]

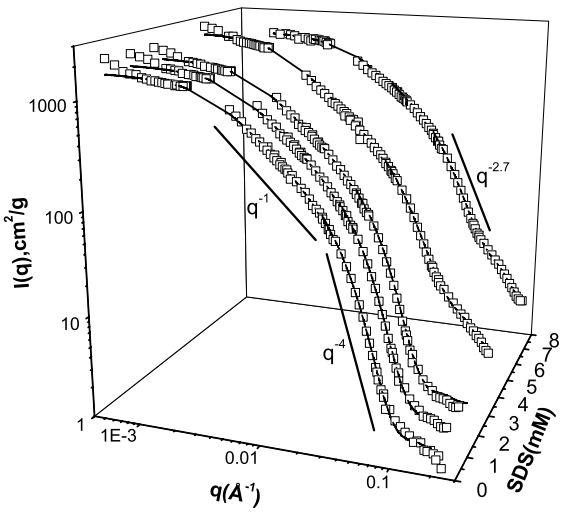

Figure 7-7. *Normalized scattering intensity as a function of scattering vector for samples with different concentrations of added surfactant. From front to back the scattering curves correspond to the following surfactant concentrations: no SDS, [SDS]= 1mM, [SDS]= 2 mM, [SDS]= 4 mM, [SDS]= 8 mM. The concentration of PEO_{45}MEMA:METAC-2 was 0.2 wt.%, and no salt was added. Individual symbols represent data obtained with SANS (q>0.005) and SLS (q< 0.004Å^{-1}). The lines represent the results from fits using models for stiff rods with elliptical cross-section (0 to 2mM), and stiff rods with elliptical cross-section and two shells (4 and 8mM).*

At high surfactant concentrations (at and above 15 mM) the shape of the scattering curves becomes more complex (Figure 7-8); presenting a shoulder at high *q*–values that is due to the presence of surfactant associated with the polyelectrolyte. It is important to point out that surface tension measurements on this system indicate that there are no free surfactant micelles present at SDS concentrations below 20 mM. Indirect Fourier transformation (IFT) analysis of these samples show that the surfactant is present in two distinct populations, one that exist as small micellar–like

aggregates associated with the polyelectrolyte and one that does not (Figure 8-3c, section 8). It is the former population that gives rise to the shoulder at high *q*–values in Figure 7-8.

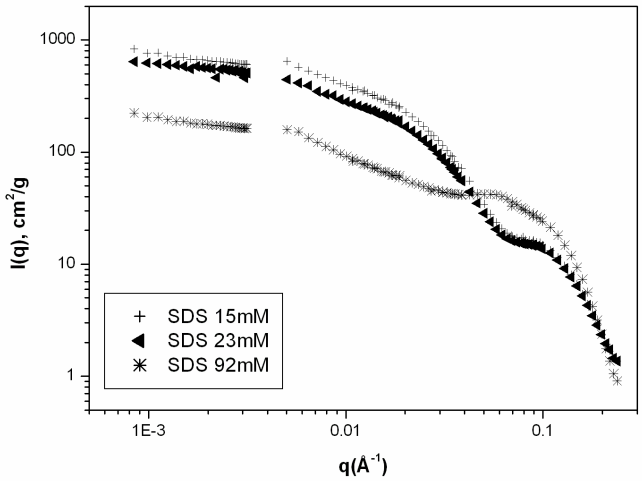

Figure 7-8. *Scattering data for $PEO_{45}MEMA$:METAC-2 samples (0.2%) in D_2O at different SDS concentrations, shown in the inset of the figure.*

7.7 Chitosan–SDS association

Pure chitosan in D_2O (0.5 weight %) adopts a Gaussian chain conformation with a persistence length of 63Å when there is not added salt, decreasing marginally to 62 Å in 30 mM of NaCl. Addition of SDS to chitosan samples results in rather complex SANS scattering curves, displaying two slopes and one Bragg–like peak. The same complex behavior is seen in samples with and without 30 mM NaCl. The Bragg–like peak is located at a characteristic distance of 37 Å, when both the SDS and chitosan contribute to the scattering. In the case where the surfactant is contrast matched, the Bragg–like peak is located at a smaller characteristic distance of 34 Å. It is not yet clear why the characteristic distance observed is different with *h*–SDS and *d*–SDS. The intensity of the peak increases with surfactant concentration, which indicates that both the chitosan and the SDS added adopted this preferred conformation.

For the sample at 30 mM NaCl, the aggregation of surfactant in specific regions on the polyelectrolyte, results in an inhomogeneous distribution of the surfactant

molecules that gives rise to a fractal conformation of the aggregates and their surfaces, at low and high surfactant concentration. This is reflected in the values of the slope at intermediate *q*–values (k2, Table 7-1), which increases from q^{-2} in absence of surfactant up to a maximum value of q^{-4} at 11.9 mM SDS. At this surfactant concentration, the distribution of the surfactant on the polyelectrolyte is such that it forms areas of homogeneous (no fractal) conformation. On the other hand, the fractal dimension of the fractal monomers in the aggregates (k1, Table 7-2) remains relatively constant with surfactant concentration.

Table 7-1. *Slopes of the scattering curves and distances calculated from the Bragg-like peaks for chitosan (Ch) samples in the presence of* h-*SDS and 30mM NaCl.*

Sample	Slope		distance(Å)
0.5%Ch, 3.0 mM SDS	k1=-2.5 0.00504 Å^{-1}<q<0.021 Å^{-1}	k2=-3.2 0.021 Å^{-1}<q<0.074 Å^{-1}	37
0.5%Ch, 5.9 mM SDS	k1=-2.6 0.00504 Å^{-1}<q<0.020 Å^{-1}	k2=-3.4 0.020 Å^{-1}<q<0.074 Å^{-1}	37
0.5%Ch, 11.9 mM SDS	k1=-2.5 0.00504 Å^{-1}<q<0.022 Å^{-1}	k2=-4.0 0.022 Å^{-1}<q<0.038 Å^{-1}	37
0.5%Ch, 23.7 mM SDS	k1=-2.6 0.00504 Å^{-1}<q<0.020 Å^{-1}	k2=-3.6 0.020 Å^{-1}<q<0.089 Å^{-1}	37
0.5%Ch, 35.6 mM SDS	k1=-2.7 0.00504 Å^{-1}<q<0.020 Å^{-1}	k2=-3.1 0.020 Å^{-1}<q<0.066 Å^{-1}	37

When there is no salt present, a similar behavior is observed, with the difference that at low surfactant concentrations (up to 5.9mM SDS), the slope of the curves at intermediate *q*–values are higher than in the 30 mM case (k2, Table 7-2). This is an indication that the aggregates formed over the distance range 50 to 160 Å are more compact. However, at higher SDS concentrations the slope in the same range is lower without the addition of salt (k2, Table 7-2). Thus, when the electrostatic interaction is

increased, the local aggregate structure becomes more compact with small additions of SDS but more expanded at higher SDS concentrations.

Table 7-2 *The slopes of the scattering curves and distances calculated from the Bragg-like peaks for chitosan (Ch) samples in the presence of h-SDS and no salt added.*

Sample	Slope		Distance(Å)
0.5%Ch, 3.0 mM SDS	k1=-2.5 $0.00504 Å^{-1}<q<0.020 Å^{-1}$	k2=-3.7 $0.020 Å^{-1}<q<0.062 Å^{-1}$	37
0.5%Ch, 5.9 mM SDS	k1=-2.5 $0.00504 Å^{-1}<q<0.020 Å^{-1}$	k2=-4.2 $0.020 Å^{-1}<q<0.054 Å^{-1}$	37
0.5%Ch, 11.9 mM SDS	k1=-2.5 $0.00504 Å^{-1}<q<0.022 Å^{-1}$	k2=-3.2 $0.022 Å^{-1}<q<0.074 Å^{-1}$	37
0.5%Ch, 23.7 mM SDS	k1=-3.3 $0.00504 Å^{-1}<q<0.047 Å^{-1}$		37
0.5%Ch, 35.6 mM SDS	k1=-2.9 $0.00504 Å^{-1}<q<0.043 Å^{-1}$	k2=-1.2 $0.043 Å^{-1}<q<0.109 Å^{-1}$	37

The main difference between the chitosan–SDS, with respect to other systems of oppositely highly charge polyelectrolytes and surfactants (e.g. PEI/SDS,[46] PCMA/SDS,[62] PVACl/SDS[84]), is that the latter systems have a q^{-4} dependence at small q–values (corresponding to compact aggregates with smooth interfaces), while in the chitosan case the slope is lower, characteristic of a fractal structure, indicating less long–range order.

8 SUMMARY OF STRUCTURES OBSERVED

Schematic representations of some of the structures described in the previous section are shown now:

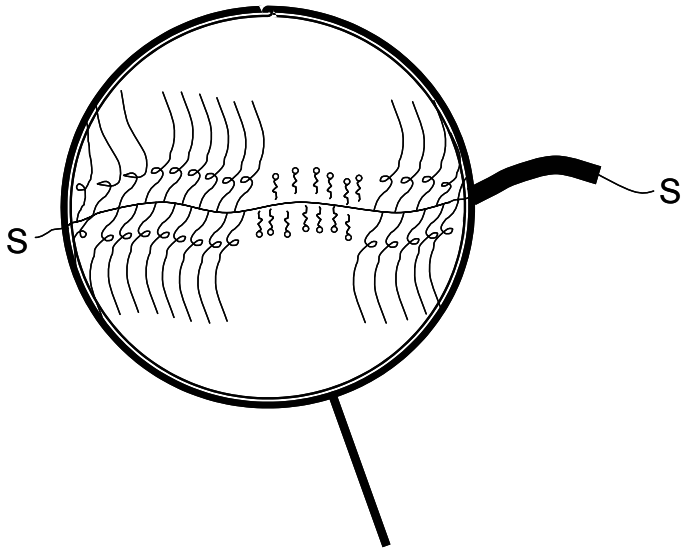

Figure 8-1. *Schematic representation of mucin monomers decorated by SDS.*

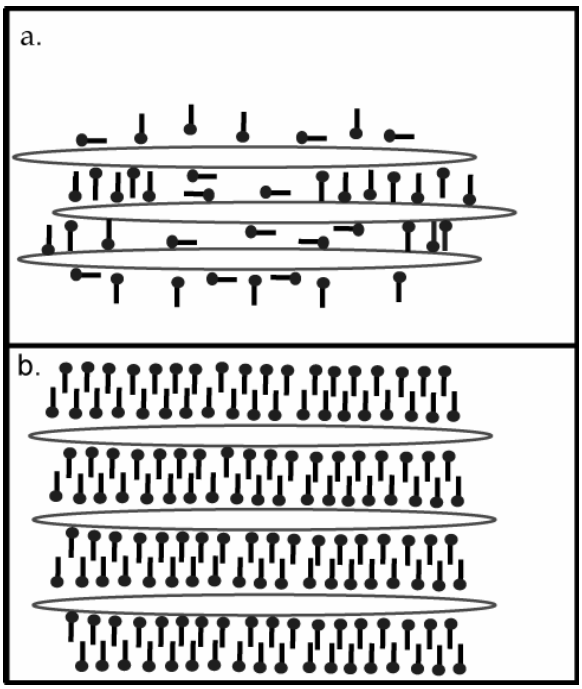

Figure 8-2. *Schematic representation of* ***a.*** *The model used to fit the SANS data of PEI/SDS aggregates at pD 10.1.* ***b.*** *The lamellar conformation of PEI/SDS aggregates at pD 4.9.*

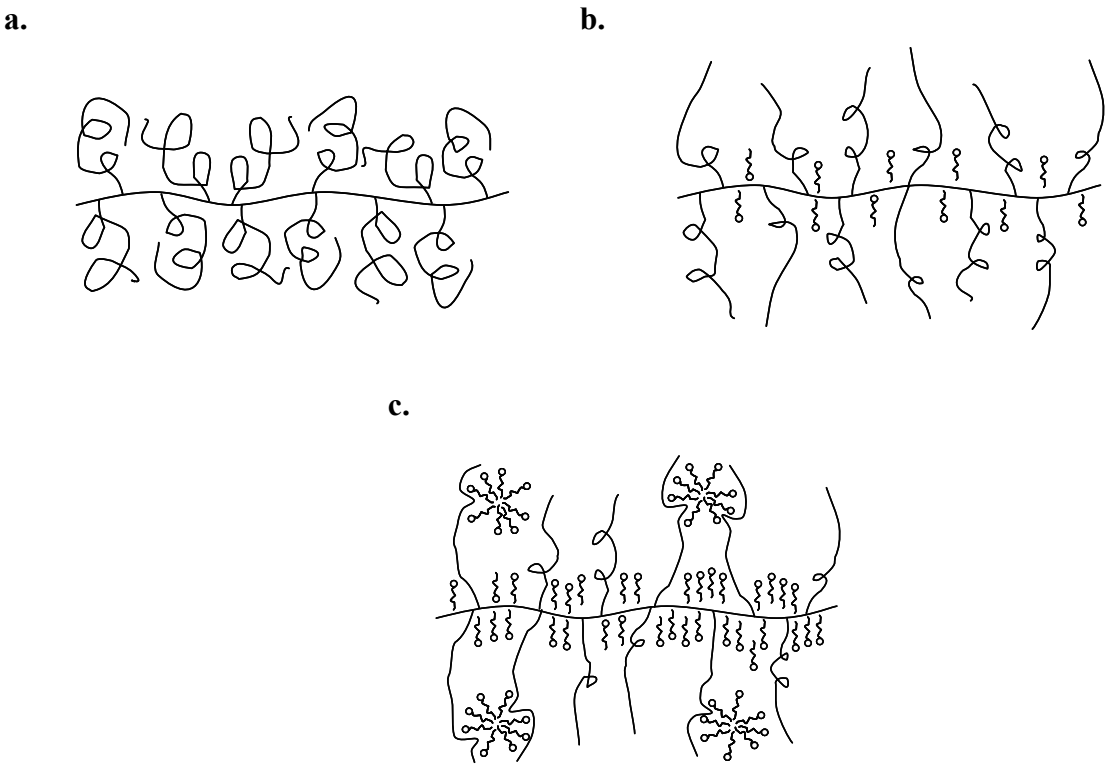

Figure 8-3. *The structure of the comb polymer (PEO_{45}MEMA:METAC-2) SDS aggregate at different surfactant concentrations.* **a.** *No added surfactant,* **b.** *below the cooperative association step,* **c.** *at saturation. The stretching of the PEO side chains is, for clarity, exaggerated in the figure.*

9 RECOMMENDATIONS FOR FUTURE WORK

The dissolution of mucin aggregates or preadsorbed mucin layers from the solid liquid interface by SDS is an indication of what this surfactant could do to the protective layers of the oral cavity or other epithelial tissues. It was show that the sugar–based surfactant (C_{12}–mal) was less effective in dissolving mucin aggregates or pre adsorbed layers from solid surfaces. It would be interesting to see how other sugar–based surfactant such as $C_{10}G_1$ and mixtures of SDS/C_{12}–mal and SDS/ $C_{10}G_1$ interact with mucin aggregates, as well as on preadsorbed mucin layers on different surfaces.

Since chitosan has also pharmaceutical and food applications, it would be interesting to see how this polyelectrolyte interacts with mucin, which would be one of the first substances it would be in contact with if administered orally. Fundamental information about these interactions could help in the development of new drug delivery systems, or better coatings for artificial parts of the body (such as tooth implants).

In the case of the methacrylate polyelectrolytes, like the PEO_{45}MEMA:METAC-2, a systematic study of the effect of varying the charge density of the polyelectrolyte, and the length of the PEO side chains on their conformation in solution as well as on their interaction with surfactants, would allow a deeper understanding of the association mechanisms between these substances.

Furthermore, continue that systematic studies of the methacrylate comb polyelectrolytes at the solid–liquid interface. Here, it would be good to investigate how this polyelectrolytes interact with different kinds of substrates, and see the effect that surfactants (e.g. SDS) have on the adsorption process and on the polyelectrolyte adsorbed layer (if any). Moreover, it would be interesting to check the effect these polyelectrolyte–surfactant systems have on the interactions between different substrates, by means of surface force techniques and tribological methods.

A deep understanding of the structural conformation of chitosan/SDS and the PEO_{45}MEMA:METAC-2/SDS aggregates could be obtained by doing SAXS measurements on these samples. The systematic study of the methacrylate polyelectrolytes should include SAXS measurements as well.

10 ACKNOWLEDGEMENTS

First of all to my supervisor Prof. Per Claesson, your passion for science has been an inspiration. Thanks for having always your door open for discussion, for your patience, for teaching me so much. We had great fun in the lab mixing samples, learning about scattering, and making surface forces measurements. It has been a pleasure to work with you.

All the people past and present from Surface Chemistry (or the Fundamental Surface Science group) especially Eva Blomberg, thanks for your unconditional help with all those little things that has to be sorted out, and for all your help with the surface force apparatus. Evgeni, we had very interesting conversations about science and other subjects, shared one office and very productive hours in the lab. Marcus Persson, we had long (productive) hours with the SFA, thanks for not loosing your patience. Ali, we shared an office for a couple of years, I think we both have learned a few things from each other; you are going to miss me. Tommaso and Mark Rutland for organizing activities with the entire group.

Everyone at YKI, especially Britt for your help in the library; Eva Sjöström and Rodrigo, for your help with the zeta sizer and other instruments. Maria Matsson, for your help with the paper work for my dissertation.

To my friends of the "Venezuelan connection", Eric and Isabel it's been great to have two of my best friends here with me during these years, thanks for all your support, I am going to miss you. Orlando, first my professor, now my friend, thanks to give me the opportunity to work with you and later to open the doors for me to come here to Sweden. Emmanuel, an adopted member of the connection. We had great fun together here in Sweden (I am also glad I did not trust my first impression on you ;-)).

To my Australian/Svensk family Mark, Arletta and little Kore. Thank you for opening the doors of your home to a disoriented Venezuelan guy in the middle of the Swedish winter. Thanks for all your help, for always been there.

My coauthors, especially Magnus Bergström and Vasil Garamus, thanks for introducing me to the world of neutron scattering and for your help with the data analysis. Robert Mészáros and Imre Varga, thanks for good scientific discussions and for you hospitality. Andra Dedinaite, for a productive collaboration and your help with the SFA. Maria Lundin, for your help with the chitosan samples, and with skiing. Joseph, we have had very interesting talks about lots of things (including science), it's been great to work with you.

To the Centre of Surfactants Based on Natural Products SNAP, for financing my project. From all the SNAP people, Ingegård Johansson from Akzo Nobel, Albert van der Waal, Tony McKee, and Donna Macnab, from Unilever Research; thanks for all the discussions and ideas you gave to this project.

A mi familia, Mama, Papa y Zaida; esta tesis se las dedico a ustedes. Sin sus enseñanzas jamás habría podido llegar tan lejos. Gracias por apoyarme en todo momento, por todo su amor y su comprensión. A mis abuelos y mi tía Kila, gracias por tenerme siempre presente en sus oraciones y al resto de mi familia, gracias por estar conmigo en todo momento, a pesar de la distancia. Los quiero y extraño muchísimo.

A mis "verdaderos amigos" Natalia, Lorea, Carlos, Rolando. A pesar de la distancia ustedes siempre han estado allí. Gracias por todas sus palabras de aliento. Por todos los momentos que compartimos. Los extraño.

11 REFERENCES

(1) Jönsson, B.; Lindman, B.; Holmberg, K.; Kronberg, B. *Surfactants and Polymers in Aqueous Solution*; JOHN WILEY & SONS, 1998.

(2) Ananthapadmanabhan, K. P. Surfactant solutions: adsorption and aggregagtion properties. In *Interactions of Surfactants with Polymers and Proteins*; Goddard, E. D., Ananthapadmanabhan, K. P., Eds.; CRC: Boca Raton, 1993.

(3) Evans, D. F.; Wennerstrom, H. *The Colloidal Domain: Where physics, Chemistry, Biology and Technology Meet*, 2nd ed.; Wiley - VCH, 1999.

(4) Kotz, J.; Kosmella, S.; Beitz, T. *Progress in Polymer Science* **2001**, *26*, 1199.

(5) Dautzenberg, H.; Jaeger, W.; Kötz, J.; Phillip, B.; Seidel, C.; Stscherbina, D. *Polyelectrolytes: Formation, characterization abd application.*; Hanser Publishers: Munich, 1994.

(6) Jorgensen, E. B.; Hvidt, S.; Brown, W.; Schillén, K. *Macromolecules* **1997**, *30*, 2355.

(7) Zhou, S.; Chu, B. *Advanced Materials (Weinheim, Germany)* **2000**, *12*, 545.

(8) Zhou, S.; Hu, H.; Burger, C.; Chu, B. *Macromolecules* **2001**, *34*, 1772.

(9) Lindman, B.; Kyrre, T. Polymer-Surfactant Interactions-Recent Developments. In *Interactions of Surfactants with Polymers and Proteins*; Goddard, E. D., Ananthapadmanabhan, K. P., Eds.; CRC Press: Boca Raton. USA., 1993; pp 427.

(10) Goddard, E. D. Polymer-surfactant interaction. Part II- Polymer and Surfactant of Opposite Charge. In *Interactions of Surfactants with Polymers and Proteins*; Goddard, E. D., Ananthapadmanabhan, K. P., Eds.; CRC Press: Boca Raton, Florida, 1993; pp 172.

(11) Zana, R. Polyelectrolyte-Surfactant Interactions: Polymer hydrophobicity, surfactant aggregation number and microstructure. In *Polymer-Surfactant systems*; Kwack, J. T. C., Ed.; Marcel Dekker Inc: New York, 1998; Vol. 77; pp 404.

(12) Shirahama, K. The nature of polymer-surfactant interactions. In *Polymer-Surfactant systems*; Kwack, J. T. C., Ed.; Marcel Dekker Inc: New York, 1998; Vol. 77; pp 143.

(13) Park, I. H.; Choi, E. *Polymer* **1996**, *37*, 313.

(14) *Light Scattering: Principles and Development*; Brown, W., Ed.; Clarendon Press and Oxford Science Publications, 1996, pp 528.

(15) Claesson, P. M.; Bergström, M.; Dedinaite, A.; Kjellin, M.; Legrand, J.-F.; Grillo, I. *Journal of Physical Chemistry B* **2000**, *104*, 11689.

(16) Cotton, J. P. Introduction to an Investigative Tool for Colloidal and Polymeric Systems. In *Neutron, X-Ray and Light Scattering.*; Lindner, P., Zemb, T., Eds.; North-Holland: Amsterdam, 1991.

(17) Wignall, G. D.; Benoit, H.; Hashimoto, T.; Higgins, J. S.; King, S.; Lodge, T. P.; Mortensen, K.; Ryan, A. J. *Macromolecular Symposia* **2002**, *190*, 185.

(18) Borsali, R. Scattering properties of ternary polymer solutions. In *Light Scattering: Principles and Development*; Brown, W., Ed.; Clarendon press: Oxford, 1996.
(19) Schillén, K.; Brown, W.; Johnsen, R. M. *Macromolecules* **1994**, *24*, 4825.
(20) Smits, R. G.; Kuil, M. E.; Mandel, M. *Macromolecules* **1994**, *27*, 5599.
(21) Sedlák, M. Structure and Dynamics of Polyelectrolyte Solutions by light Scattering. In *Physical Chemistry of Polyelectrolytes*; Radeva, T., Ed.; Marcell Dekker, Inc.: New York, 2001; Vol. 99.
(22) Ionescu, L.; Picot, C.; Duval, M.; Duplessix, R.; Benoit, H.; Cotton, J. P. *Journal of Polymer Science, Polymer Physics Edition* **1981**, *19*, 1019.
(23) Stuhrmann, H. B. *Journal of Applied Crystallography* **1974**, *7*, 173.
(24) Cabane, B.; Duplessix, R. *Colloids and Surfaces* **1985**, *13*, 19.
(25) BrunnerPopela, J.; Glatter, O. *Journal Of Applied Crystallography* **1997**, *30*, 431.
(26) Magid, L. J. *Journal of Physical Chemistry B* **1998**, *102*, 4064.
(27) Bohidar, H. B. Characterization of polyelectrolytes by dynamic light scattering. In *Handbook of Polyelectrolytes and Their Applications*; Tripathy, S. K., Kumar, J., Nalwa, H. S., Eds.; American Scientific Publishers: Stevenson Ranch, 2002; Vol. 2; pp 117.
(28) *Scattering in Polymeric and Colloidal Systems*; Brown, W.; Mortensen, K., Eds.; Gordon and Breach Science Publishers: Amsterdam, 2000.
(29) Hammouda, B. "A tutorial on Small-Angle Neutro Scattering from Polymers," National Institute of Standards and Technology, 1995.
(30) Bud, P. M. Determination of molar masses of polyelectrolytes. In *Handbook of polyelectrolytes and their applications*; Tripathy, S. K., Kumar, J., Nalwa, H. S., Eds.; American Scientific Publishers: Stevenson Ranch, 2002; Vol. 2; pp 91.
(31) Hiemenz, P. C.; Rajagopalan, R. *Principles of colloid and surface chemistry: Third edition, revised and expanded*; Marcel Dekker, Inc: New York, 1997.
(32) Rabek, J. F. *Experimental methods in polymer chemistry*; John Wiley & Sons: Chichester, 1980.
(33) Fleer, G. J.; Cohen-Stuart, M. A.; Scheutjens, J. M. H. M.; Vicent, B. *Polymers at interfaces*; Chapman & Hall: London, 1993.
(34) Brown, W. *Scattering Methods: A Brief Introduction*; Department of Chemistry. University of Uppsala: Uppsala.
(35) Koppel, D. E. *Journal of Chemical Physics* **1972**, *57*, 4814.
(36) King, S. Small-angle Neutron Scattering. In *Modern Techniques for Polymer Characterization*; Pethrick, R. A., Dawkins, J. V., Eds.; John Wiley &Sons Ltd: Chichester, 1999; pp 171.
(37) Pedersen, J. S. Instrumentation for small-angle scattering. In *Modern aspects of small-angle scattering*; Brumberger, H., Ed.; Kluwer Academic Publishers, 1995.
(38) Arrighi, V. Neutron scattering studies of polymer dynamics. In *Modern techniques for polymer characterization*; Pethrick, R. A., Dawkins, J. V., Eds.; John Wiley & Sons: Chichester, 1999.

(39) Bates, R. G. *Determination of pH: Theory and practice*, First ed.; John Wiley and Sons, Inc.: New York, 1964.
(40) Glasoe, P. K.; Berson, L. *Journal of Physical Chemistry* **1964**, *68*, 1560.
(41) Krezel, A.; Bal, W. *Journal of Inorganic Biochemistry* **2004**, *98*, 161.
(42) Glatter, O. *Journal of Applied Crystallography* **1980**, *13*, 577.
(43) Glatter, O. *Journal of Applied Crystallography* **1977**, *10*, 415.
(44) Pedersen, J. S. *Advances In Colloid And Interface Science* **1997**, *70*, 171.
(45) Ahad, E.; Jennings, B. R. *Journal of Physics D. Applied Physics* **1970**, *3*, 1509.
(46) Bastardo, L. A.; Garamus, V. M.; Bergström, M.; Claesson, P. M. *Journal of Physical Chemistry B* **2005**, *109*, 167.
(47) Gunnarsson, G.; Jönsson, B.; Wennerström, H. *J. Phys. Chem.* **1980**, *84*, 3114.
(48) Rosen, M. J. *Surfactants and Interfacial Phenomena*; John Wiley & Sons: New York, 1989.
(49) Hines, J. D.; Thomas, R. K.; Garrett, P. R.; Rennie, G. K.; Penfold, J. *Journal of Physical Chemistry B* **1998**, *102*, 9708.
(50) Nilsson, F.; Söderman, O.; Hansson, P.; Johasson, I. *Langmuir* **1998**, *14*, 4050.
(51) Carlstedt, I.; Sheehan, J. K.; Corfield, A. P.; Gallagher, J. T. *Essays of Biochemistry* **1985**, *5*, 40.
(52) Shogren, R.; Jamieson, A. M.; Blackwell, J.; Jentoft, N. *Biopolymers* **1 986**, *25*, 1505.
(53) *Saliva and Oral Health*; Second ed.; Edgar, W. M.; O'Mullane, D. M., Eds.; British Dental Association: London, England, 1996.
(54) Shi, L.; Caldwell, K. D. *Journal of Colloid and Interface Science* **2000**, *224*, 372.
(55) Carlstedt, I. *From the Department of Physiological Chemistry, University of Lund* **1988**.
(56) Bettelheim, F. A.; Scheinthal, B. M. *J. Polymer Sci.* **1970**, *30*, 117.
(57) Mészáros, R.; Thompson, L.; Bos, M.; Varga, I.; Gilányi, T. *Langmuir* **2003**, *19*, 609.
(58) Winnik, M. A.; Bystryak, S. M.; Chassenieux, C. *Langmuir* **2000**, *16*, 4495.
(59) Bloys van Treslong, C. J.; Staverman, A. J. *Recueil des Travaux Chimiques des Pays-Bas* **1974**, *93*, 171.
(60) Li, Y.; Ghoreishi, J.; Warr, J.; Bloor, D. M.; Holzwarth, J. F.; Wyn-Jones, E. *Langmuir* **2000**, *16*, 3093.
(61) Iruthayaraj, J.; Poptoshev, E.; Vareikis, A.; Makuska, R.; van der Wal, A.; Claesson, P. M. *Macromolecules* **2005**, *28*, 6152.
(62) Claesson, P. M.; Ninham, B. W. *Langmuir* **1992**, *8*, 1406.
(63) Rinaudo, M.; Domard, A. Solution properties of chitosan. In *Chitin and chitosan*; Skjåk-Braek, G., Anthonsen, T., Sandford, P., Eds.; Elsevier Science Publishers LTD: London, 1989; pp 71.
(64) Rinaudo, M.; Milas, M.; Le Dung, P. *International Journal of Biological Macromolecules* **1993**, *15*, 281.
(65) Shahidi, F.; Abuzaytoun, R. *Advances in food and nutrition research* **2005**, *49*, 93.

(66) Thongngam, M.; McClements, D. J. *Journal of Agricultural and Food Chemistry* **2004**, *52*, 987.
(67) Brown, W. *Light Scattering: Principles and Development*; Clarendon Press and Oxford Science Publications: Oxford, 1996.
(68) Huglin, M. B. *Light scattering from polymer solutions*; Academic Press: London, 1972.
(69) Dijt, J. C.; Cohen-Stuart, M. A.; Fleer, G. J. *Advances in colloids and interface science* **1994**, *50*, 79.
(70) Israelevich, J. *Intermolecular and Surface Forces.*, Second ed.; Academic Press: San Diego. USA., 1992.
(71) Kumpulainen, A. Interfacial properties of some carbohydrate based surfactants and polymers: Experiments and theory, Royal Institute of Technology, KTH, 2004.
(72) Vainshtein, B. K. *Diffraction of X-Rays by chain molecules*; Elsevier: Amsterdam, 1966.
(73) Pettersson, E. T. Charged colloids observed by electrophoretic and diffusion NMR, Royal Institute of Technology, KTH, 2005.
(74) Binning, G.; Rohrer, H.; Gerber, C.; Weibel, E. *Physical Review Letters* **1982**, *49*, 57.
(75) Feiler, A.; Larson, I.; Jenkings, P.; Attard, P. *Langmuir* **2000**, *16*, 10269.
(76) Skoog, D. A.; Leary, J. J. *Análisis instrumental*; McGraw Hill Interamericana: Madrid, 1994.
(77) Mörnstam, B.; Whlund, K.-G.; Jönsson, B. *Analytical Chemistry* **1997**, *69*, 5037.
(78) Sedlák, M. *Langmuir* **1999**, *15*, 4045.
(79) Brown, W.; Fundin, J.; Maria da Graça, M. *Macromolecules* **1992**, *25*, 7192.
(80) Cabane, B.; Duplessix, R. *J. Physique* **1982**, *43*, 1529.
(81) Claesson, P. M.; Dedinaite, A.; Poptoshev, E. Polyelectrolyte-Surfactant Interactions at Solid -Liquid Interfaces Studied with Surface Force Techniques. In *Physical Chemistry of Polyelectrolytes*; First ed.; Radeva, T., Ed.; Marcel Dekker, Inc.: New York. USA, 2001; pp 882.
(82) Bergström, L. M.; Kjellin, U. R. M.; Claesson, P. M.; Grillo, I. *Journal of Physical Chemistry B* **2004**, *108*, 1874.
(83) Li, Y.; Xu, R.; Couderc, S.; Bloor, D. M.; Warr, J.; Penfold, J.; Holzwarth, J. F.; Wyn-Jones, E. *Langmuir* **2001**, *17*, 5657.
(84) Bergström, M.; Kjellin, U. R. M.; Claesson, P. M.; Pedersen, J. S.; Nielsen, M. M. *journal of Physical Chemistry B* **2002**, *106*, 11412.
(85) Katz, J. J. Deuterium and Tritium. In *Kirk-Othmer Encyclopedia of Chemical Technology*; Kirk, R. E., Othmer, D. F., Eds.; John Wiley and Sons, Inc: New York, 2004.
(86) Ericsson, C. A.; Söderman, O.; Garamus, V. M.; Bergström, M.; Ulvenlund, S. *Langmuir* **2004**, *20*, 1401.
(87) Whiddon, C.; Soderman, E. *Langmuir* **2001**, *17*, 1803.
(88) Bergström, L. M.; Bastardo, L. A.; Garamus, V. M. *Journal of Physical Chemistry B* **2005**, *109*, 12387.
(89) Hammouda, B.; Ho, D.; Kline, S. *Macromolecules* **2002**, *35*, 8578.
(90) Shirota, H.; Horie, K. *Macromolecular Symposia* **2004**, *207*, 79.

(91) Bastardo, L. A.; Mészáros, R.; Varga, I.; Gilányi, T.; Claesson, P. *Journal of Physical Chemistry B* **2005**, *109*, 16196.
(92) Kabanov, A. V.; Bronich, T. K.; Kabanov, V. A.; Yu, K.; Eisenberg, A. *Journal of the American Chemical Society* **1998**, *120*, 9941.
(93) Jayachandran, K. N.; Maiti, S. *Polymer* **2002**, *43*, 2349.
(94) Nisha, C. K.; Basak, P.; Manorama, S. V.; Maiti, S.; Jayachandran, K. N. *Langmuir* **2003**, *19*, 2947.

APPENDIX 1: SCATTERING LENGTH DENSITIES USED

Table 0-1. *Average scattering length density per unit mass of the solutes employed in SANS measurements in D_2O.*

Component	$\Delta\rho$ (cm/g)
h–SDS	-5.14×10^{10}
d–SDS	0.33×10^{10}
$C_{10}G_1$*	-4.43×10^{10}
PEI	-3.09×10^{10}
PEO_{45}MEMA:METAC-2	-4.80×10^{10}
Chitosan	-5.75×10^{10}

* Assuming that four hydrogen atoms sitting on each OH group of the glucose headgroup are all exchanged with deuterium atoms from the solvent D_2O molecules.[87]

APPENDIX 2: LIST OF ABBREVIATIONS USED

cmc	Critical micellar concentration
$C_{10}G_1$	*n*-decyl β-D-glucopyranoside
$C_{12}E_5$	Penta(oxyethylene) dodecyl ether
C_{12}-mal	*n*-dodecyl β-D-maltopyranoside
D_2O	Heavy water
d–SDS	Deuterated sodium dodecyl sulfate
h –SDS	Hydrated sodium dodecyl sulfate
NMR	Nuclear magnetic resonance
PEI	Polyethylene imine
PEO	Polyethylene oxide
PEO_{45}MEMA:METAC-2	Poly(ethylene oxide) monomethylether methacrylate methacryloxyethyl trimethylammonium chloride
SANS	Small–angle neutron scattering
SDS	Sodium dodecyl sulfate
SLS	Static light scattering